



School of Engineering Technology

Capstone Project Proposal

Designing and Implementing of Smart and Power Efficient Wireless Charger for Electric Vehicles.

Students:

- Nadine Al-Jada - 60105890
- Islam Azzam - 60105790

Supervisor: Hassan Mahasneh

Course instructor: Zeina

Data: 7 / 4 / 2025

DECLARATION STATEMENT

We, undersigned students, hereby declare that this project report and work described in this report is entirely our own work and has not been copied from any other source. Any material that has been used from other sources has been cited and acknowledged in proper style.

We are totally aware that any copying or improper citation of references/sources used in this report will be considered plagiarism, which is a clear violation of Academic Dishonesty Policy at the University of Doha for Science and Technology (UDST).

	Student Name	Student ID	Signature	Date
1	Nadine Al-Jada	60105890		
2	Islam Azzam	60105790		

Abstract

This applied project aims to develop a smart and power-efficient wireless charging mechanism for electric vehicles. The project is divided into two main parts: wireless charger design and autonomous mechanism design.

In the wireless charger design, the project targets achieving a power-efficient system by examining the effects of different coil geometries and sizes, exploring various coil materials, adjusting the number of coil turns, and varying the gaps between coils. These factors are meticulously tuned to optimize power efficiency.

In the autonomous mechanism design, the focus is on developing an autonomous system where a small robotic vehicle, equipped with a transmitting plate, navigates precisely to align with the vehicles' receiving plate. The design also incorporates collision and obstacle avoidance mechanisms, enabling the vehicle to detect and navigate around obstacles smoothly to reach its destination.

This project demonstrates the potential for integrating smart autonomous systems with wireless charging technologies to enhance the efficiency and convenience of electric vehicles charging solutions.

ACKNOWLEDGEMENTS

We would like to thank our supervisor, Hassan Mahasanneh, for his continuous supervision, constructive criticism, and encouragement during the preparation of this project

Table of Contents

Chapter 1: Introduction	1
1.1 Background & Motivation	2
1.2 Problem Statement	3
1.3 Objectives	4
Chapter 2: Literature Review	5
2.1 Review of Related Work	5
2.2 Technical Background	6
2.3 Benchmarking criteria	7
2.4 Benchmarking comparison table	
Chapter 3: Project Requirements and Specifications	7
3.1 Customer Needs	7
3.2 User Experience	8
3.3 System Requirements	9
3.3.1 Software	9
3.3.2 Performance	9
3.3.3 Safety	9
3.4 Functional Modeling update flowchart islam islam islam	9
3.5 Functional & Non-Functional Requirements.	11
3.6 Design Constraints	11
3.6.1 Time Constraint	12
3.6.2 Budget Constraints	12
3.6.3 Availability of Components	12
3.6.4 Technical Constraints	12
3.6.5 Testing and Experimental Constraints	13
3.7 Ethical, Safety, and Environmental Considerations	13
3.7.1 Ethical consideration	13
3.7.2 Safety Constraints	13
3.7.3 Environmental Constraints	13
3.8 Standards and Regulations	13
3.9 Risk assessment and mitigation	14
Chapter 4: Methodology & Design Approach	0
4.1 Hardware Design Approach	0
4.1.1 Compensation topology	0
4.1.2 Coil misalignment	6
Autonomous Alignment Mechanism	12
4.2 Software Design Approach	12

4.2.1 Available Homing Solutions	13
Comparison of Homing Solutions for Autonomous Alignment	13
4.2.3 RF Beacon Design	14
4.2.3.1 Signal Strength Homing	14
4.2.3.2 Triangulation Homing	14
4.2.3.3 Comparison of Techniques	15
4.2.4 Comparison of Robotic Frameworks	15
4.2.5 Comparison of LIDAR-Based Obstacle Avoidance Algorithms	16
4.2.6 Programming Languages and Tools	17
4.2.7 Signal Strength Homing System (Navigation Phase)	19
4.2.8 Full Software Design Approach	20
4.3 List of required components	22
4.4 Calculations and Modeling	24
4.5 Expected Deliverables	27
4.5.1 Capstone 1 Deliverables	27
4.5.2 Capstone 2 Deliverables	27
4.6 Project Planning	30
4.7 Project budget	30
4.8 Project Management	31
Chapter 5: Preliminary Results and Findings	0
5.1 Prototype Development	0
5.2 Simulation & Testing Results.	0
6 References	3

List of Appendices

Appendix A	63
Appendix B	63
Appendix C	63
Appendix D	63
Appendix E	64
Appendix F	64
Appendix G	64
Appendix H	64
Appendix I	64
Appendix J	64
Appendix K	65
Appendix L	65

List of Figures

Fig.1 Conventional Wireless EV Charging Process.	2
Fig.2 Inductive Power Transfer (IPT) Block Diagram.	3
Fig.3 (a) Conventional Wireless EV Charging Mechanism , (b) Proposed Autonomous Mechanism.	4
Fig.4 System Software Functional Model	12
Fig.5 Compensation Networks: (a) Series-Series (SS). (b) Series-Parallel (SP). (c) Parallel-Series (PS). (d) Parallel-Parallel (PP)	22
Fig.6 Model of (a) spiral, (b) DD, and (c) solenoid coil structures.	24
Fig.7 Design of the bipolar pad (BPP) pad showing the major dimensions	25
Fig. 8 Signal Strength Homing Flowchart	39
Fig.9 Full Autonomous System Flowchart	41
Fig.10 Gantt Chart	50
Fig.11 Gain Plot (a) Directivity Plot (b)	54
Fig.12 Simulation Directivity Pattern	54
Fig.13 VSWR Plot	55
Fig.14 Robot Initial Model	56
Fig.15 Autonomous Simulation	56

List of Tables

Tab. 1: Comparison of existing charger systems/ autonomous.....	9
Tab. 2: EV Charger Classification.....	16
Tab. 3: Risk assessment and mitigation.....	16
Tab. 4 : Comparison of Homing Solutions for Autonomous Alignment.....	34
Tab. 5: Formulas Table.....	45
Tab. 6: Work breakdown Structure.....	48
Tab. 7: Components Pricing.....	51

LIST OF ABBREVIATIONS

Abbreviation	Meaning
AC	Alternating Current
ADC	Analog-to-Digital Converter
DC	Direct Current
DD	Double D
DWA	Dynamic Window Approach
EMF	ElectroMotive Force
EMI	Electromagnetic Interference
EV	Electric Vehicles
GPIO	General Purpose Input Output
HF	High Frequency
ICNIRP	International Commission on Non-Ionizing Radiation Protection
IEC	International Electrotechnical Commission
IEEE	Institute of Electrical and Electronics Engineers

IGBT	Insulated-Gate Bipolar Transistor
IPT	Inductive Power Transfer
IR	Infrared Sensors
KCL	Kirchhoff's Current Law
KVL	Kirchhoff's Voltage Law
LiDAR	Light Detection And Ranging
LoS	Line of Sight
MOSFET	Metal Oxide Semiconductor Field-Effect Transistor
MQTT	Message Queuing Telemetry Transport
PP	Parallel-Parallel
PS	Parallel-Series
PTE	Power Transfer Efficiency
PWM	Pulse Width Modulation
QDQ	Quad D Quadrature
RF-Beacon	Radio Frequency Beacon
RFID	Radio Frequency Identification
ROS	Robotic Operating systems
RSSI	Received Signal Strength Indicator
SAE	Society of Automotive Engineers

SDG	Sustainable Development Goals
SLAM	Simultaneous Localization and Mapping
SP	Series-Parallel
SS	Series-Series
UDST	University of Doha for Science and Technology
VHF	Vector Field Histogram
WPT	Wireless Power Transfer
YARP	Yet Another Robot Platform
ZVS	Zero Voltage Switching

1 Chapter 1: Introduction

Electric vehicles (EVs) have witnessed remarkable advancements in performance and technology, leading to their rapid adoption [1]. Regardless, most EVs still rely on conventional cable-based charging. The need for effective, practical charging options is increasing along with the number of EVs on the road. However, there are a number of limitations to traditional charging techniques. These solid connections can spark while plugging and unplugging, which limits their use in sensitive locations like airports and areas close to petrol stations, as it poses safety hazards, especially in poor weather, in addition to, inconvenience for people with disabilities making it inaccessible for individuals with mobility impairments. These difficulties have sparked interest in wireless charging solutions, which provide a more secure, adaptable, and convenient option [2, page1-2], Which can be overcomed using the technology of wireless power transfer (WPT), specifically inductive power transfer (IPT), where a transmitter coil generates a magnetic flux, inducing a voltage in a receiver coil that charges the battery which helped to overcome drawbacks like low efficiency and limited range. Charging efficiency using WPT is affected by factors like coil geometry, material, alignment, and space between coils.

The autonomous system plays a crucial role in enhancing wireless charging efficiency by addressing misalignment issues and reducing the energy loss. The robot will use sensors to detect obstacles and ensure a smooth approach, improving user convenience and reliability. This level of automation is essential for future smart cities and infrastructure, where seamless, hands-free charging solutions will be necessary for widespread EV adoption.

This multidisciplinary research aims to overcome these limitations by developing a smart, power-efficient wireless charging system for EVs, integrating two key components, First, optimizing coil geometries, materials, and configurations to enhance charger performance. Then, an autonomous robotic system will be developed to carry the transmitter plate, precisely align it with the EV's receiver, and minimize the gap for optimal charging. The robotic system will also incorporate collision and obstacle avoidance features to ensure seamless operation assisting in the worldwide shift to environmentally friendly transportation.

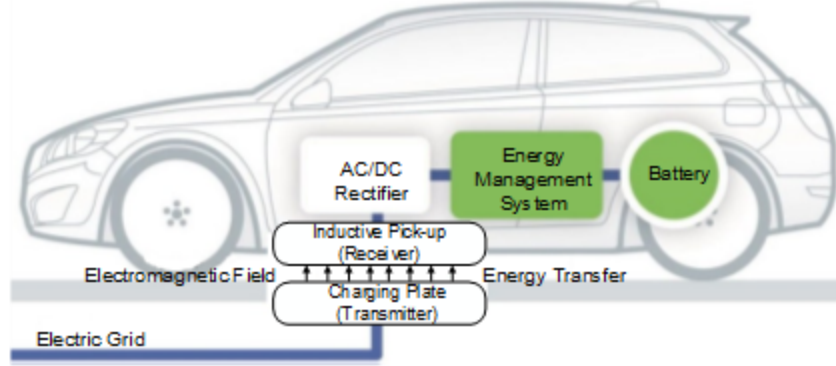


Fig.1 Conventional Wireless EV Charging Process.

1.1 Background & Motivation:

The rapid adoption of EVs marks a critical shift toward sustainable transportation, driven by global efforts to reduce greenhouse gas emissions. However, conventional wired charging systems pose significant challenges, including safety risks from sparking during plugging/unplugging, accessibility barriers for individuals with disabilities, and inefficiencies caused by connector wear. These limitations have spurred interest in wireless charging technologies, which eliminate physical connections and offer greater convenience [27, page 2].

Wireless Power Transfer (WPT), first conceptualized by Nikola Tesla in the late 19th century, has evolved into a viable solution for EV charging. Modern WPT systems fall into two categories [3]:

1. **Near-field WPT:** Operates over short distances using EM induction (inductive coupling) or electric fields (capacitive coupling).
2. **Far-field WPT:** Transmits energy over longer distances using technologies like microwaves or lasers, requiring strict LoS conditions.

For EV applications, IPT dominates due to its balance of efficiency and practicality [3]. In IPT systems, see Fig. 2, a transmitter coil generates a high-frequency alternating magnetic field, inducing a voltage in a receiver coil embedded in the EV. Efficiency depends on factors like coil alignment, geometry, and the gap between coils (typically 140–210 mm) [4].

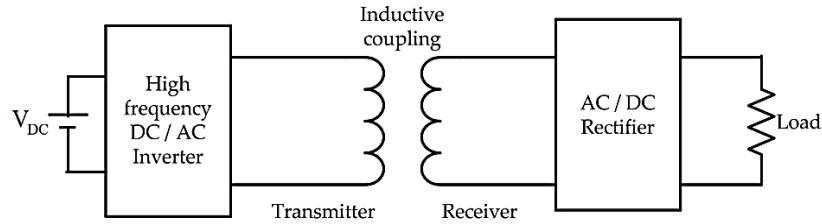


Fig.2 Inductive Power Transfer (IPT) Block Diagram.

Despite advancements, existing systems face critical limitations:

- Misalignment sensitivity: Even minor misalignment reduces efficiency by up to 30%.
- Driver dependency: Manual parking precision is required, leading to user frustration.
- Static infrastructure: Fixed ground plates lack adaptability to dynamic environments.

Autonomous Alignment Mechanism

To address these challenges, this project integrates an autonomous robotic system (Figure 3b) with resonant coupling technology. The robotic car, equipped with a transmitter plate, uses an RF-Beacon based homing system operating between 3.5 GHz to 6.5 GHz to navigate toward the EV's receiver plate [5], important characteristics include:

1. Precision Alignment.
2. Gap Minimization.
3. Collision Avoidance.

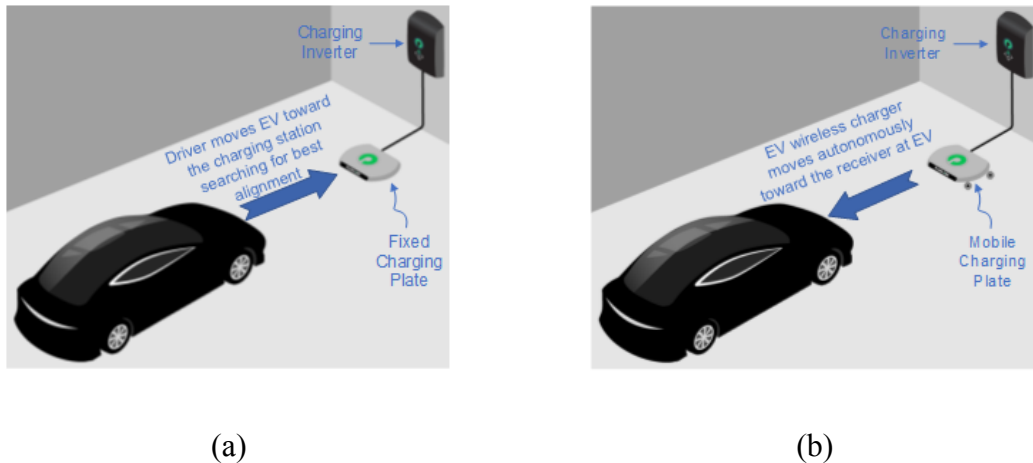


Fig.3 (a) Conventional Wireless EV Charging , (b) Proposed Autonomous Mechanism.

1.2 Problem Statement

Existing wireless EV charging systems rely on static transmitter plates, requiring drivers to park with millimeter-level precision. Misalignment between the transmitter and receiver coils reduces efficiency by up to 30% [6], while time-consuming and prone to errors. Additionally, conventional systems lack adaptability to dynamic conditions and struggle with EMI.

Key Issues: Driver dependency and hazards.

1. Driver dependency for precise alignment with the charger.
2. Inaccessibility for disabled people for traditional plug chargers.
3. Power loss due to coil misalignment and gap variations.

1.3 Objectives

This project aims mainly to develop a smart and power efficient wireless charging mechanism for EV's. This can be achieved through two broad streams: wireless charger design and autonomous mechanism design.

1. Wireless charger design:

- 1.1. Comparative analysis of WPTS technologies by evaluating each for efficiency, cost, scalability and complexity.
- 1.2. Compensation topology optimization by designing and testing each type, and fields of use under specific load variations while still achieving 80% end-to-end efficiency at 10 cm air gap.
- 1.3. Coil design selection by comparing various coil configurations to determine optimal coupling coefficients k and mutual inductance M at air gaps of 10 cm.
 - 1.3.1. Initial prototype on selected geometry and test multi-layer coil designs (2–5 layers) to enhance magnetic flux density while minimizing eddy current losses
 - 1.3.2. Quantify the impact of coil aspect ratio on misalignment tolerance ± 15 cm lateral and power transfer efficiency.

- 1.4. Experiment with air gaps 5–30 mm and lateral misalignment 0–20 cm to characterize efficiency drop to reach a target of $\leq 10\%$ loss at 15 cm.
- 1.5. Integrate ferrite cores or metamaterials to reduce flux leakage and improve coupling coefficient to achieve $k \geq 0.4$.
- 1.6. Optimize coil and balance tradeoffs to compensate for the autonomous weak points.

2. Autonomous Mechanism Design:

- 2.1. Design a small 4-wheeled robotic car installed with a transmitting plate that is equipped with differential steering, move freely and with maximum positioning accuracy
- 2.2. Enable the car to autonomously align and connect its transmitting plate with the receiver plate on an EV using hybrid localization system ensuring precise positioning with alignment accuracy of ≤ 2 cm between plates.
- 2.3. Implement obstacle avoidance while maintaining energy efficient navigation and path mapping

2 Chapter 2: Literature Review

2.1 Review of Related Work: Existing research, designs, or products related to the project.

Researchers and industry innovators have long tackled the challenge of efficient EV charging, and recent efforts have increasingly focused on wireless solutions that overcome the limitations of conventional cable-based systems. Early work in the field concentrated on developing the core technology of WPT. For example, companies like EV Safe Charge introduced the ZiGGY robotic mobile charging platform, which revolutionized the charging process by using an autonomous device to navigate parking lots and deliver on-demand charging. EV Safe Charge demonstrated that mobile charging systems could eliminate the need for extensive infrastructure modifications and specialized parking spaces, while also offering additional benefits such as integrated advertising [7].

In the same way, Bumper Charger addressed the practical shortcomings of existing wireless charging methods through its Car Charging Robot. Bumper Charger highlighted that approximately 20% of EV owners reverted to gasoline vehicles because of inconvenient and

slow charging processes. Their automated, hands-free charging solution, which requires no fixed installation, actively locates a parked EV and initiates the charging process, addressing both user convenience and infrastructure limitations [9].

More recent academic research has further advanced the field by integrating autonomous technologies with wireless charging systems [1]. Developed a vision-based autonomous charging system that employs computer vision and machine learning. Their work shows that precise alignment between the charging unit and the EV's receiver is critical for maximizing energy transfer efficiency, as minor misalignments can lead to significant energy losses. This study reinforces the idea that autonomous positioning systems are not merely an add-on but a fundamental component for enhancing charging performance. Concurrently, reviewed advances in wireless charging technology, focusing on improvements in IPT systems. Their work emphasizes that the efficiency of wireless charging relies heavily on the design of transmitter and receiver coils, specifically their geometry, material, and alignment. They argue that integrating optimized IPT designs with autonomous positioning systems can address the dual challenges of energy loss and installation complexity in modern EV charging infrastructures [9].

Overall, these studies establish a clear progression; where early work focuses on the technical functionals of WPT, while the more recent work focuses on the autonomous navigation to overcome misalignment and accessibility.. This literature review lays the groundwork for the current project, which aims to combine advanced IPT techniques with an autonomous robotic vehicle to create a smart, power-efficient wireless charging system for EVs. By combining academic research and industry practices, the project aims to contribute a solution that is both efficient and user-friendly, paving the way for more adaptable and widespread EV charging infrastructure.

2.2 Technical Background: Key theories, principles, and technologies involved.

The first part of this project is based on Faraday's Law of Electromagnetic Induction, which states that a changing magnetic field generates an electromotive force (EMF) in a nearby conductor, represented as $\varepsilon = d\varphi_b/dt$. This principle controls inductive coupling between the Tx and Rx [10], as the Tx coil's 85 kHz AC current creates a fluctuating magnetic field that induces a current in the Rx coil. Maxwell's Equations describe the electromagnetic interactions;

additionally, Ampere's Law $\nabla \times H = J + \partial D / \partial t$ describes how the Tx coil's current (J) and time-varying electric field ($\partial D / \partial t$) produce a magnetic field (H), with $B = \mu_0 \mu_r H$ enhanced by the ferrite core $\mu_r \approx 2000$. This magnetic field induces a current in the Rx coil per Faraday's Law, enabling power transfer [28].

Furthermore, Laws of Magnetism, encapsulated within Maxwell's Equations, specially Gauss's Law for Magnetism and Ampere's Law, which states that the behavior of magnetic fields is critical to IPT. Gauss's Law for Magnetism ($\nabla \cdot B = 0$) explains that magnetic field lines form closed loops, ensuring that the magnetic flux generated by the Tx coil remains continuous [12].

Kirchhoff's Current Law (KCL) points that the sum of currents entering a node = the sum of currents leaving it, shown in $\sum I_{in} = \sum I_{out}$, ensuring charge conservation, for balancing current distribution in rectifier and inverter circuits handling grid AC to DC conversion. Kirchhoff's Voltage Law (KVL) states that the algebraic sum of all voltage drops around a closed loop equals zero, or $\sum V = 0$, reflecting energy conservation [13].

The autonomous system depends on RSSI comparison for the homing navigation using the Friis transmission equation:

$$Pr = P_t G_t G_r \left(\frac{\lambda}{4\pi d} \right)^2$$

where P_r is the received power, P_t is the transmitted power, G_t and G_r are the gains of the transmitting and receiving antennas, λ is the wavelength, and d is the distance, allowing the robot to know the direction of the EV's receiving plate by comparing the RSSI values from three or more different receivers [14].

2.3 Benchmarking criteria

- 2.3.1 Alignment Accuracy (cm): Measures the precision of the system in aligning the Tx and Rx plates, targeting $\pm 5\text{--}10$ cm to ensure efficient WPT.
- 2.3.2 WPT Efficiency (%): Assesses power transfer efficiency at 85 kHz, 3.7 kW, aiming for 85% at 5 cm air gap.
- 2.3.3 Response Time (ms): Evaluates the speed of detecting and avoiding obstacles, targeting < 100 ms for real-time performance.
- 2.3.4 Misalignment Tolerance (mm): Measures the system's ability to maintain efficiency under lateral misalignment, target > 80% efficiency at 15cm offset.

2.4 Benchmarking comparison table

Table 1

Comparison of existing charger systems/ autonomous

Criterion	Traditional Wired Charging (Level 2)	Static Wireless Charging	Proposed solution
Alignment Accuracy (cm)	N/A	10 cm	5-10cm
WPT Efficiency (%)	95%	90%	92%
Response Time (ms)	N/A	N/A	150 ms
Misalignment Tolerance (mm)	N/A	100 mm	100 mm

3 Chapter 3: Project Requirements and Specifications

3.1 Customer needs

Our solution targets EV owners who are looking for a convenient and reliable wireless charging at home, meeting their particular requirements in a domestic setting. Owners prioritize convenience, automation and hands-free charging , where the system

automatically aligns the charging plate ($\pm 5\text{--}10$ cm accuracy) and charges automatically in their garage. They require efficiency as well as speed, delivering power with 80% efficiency at 3.7 kW to charge a standard 60 kWh EV battery in 16–20 hours, the same as Level 2 wired charging. Cost-effectiveness is what homeowners value most, and a system cost of $\leq \$2.5K$ QAR to be an affordable alternative for home use. Safety is the priority, with owners wanting overcurrent protection, automatic thermal fault shutdown ($>85^\circ\text{C}$), and contact detection (>5 N force), as well as real-time feedback via a smartphone application to guard against safe operation. Last but not least, compatibility with a large number of EV models enables the system to be flexible in meeting many different user demands and future automobile upgrades.

3.2 User Experience

Focuses on how the end user or parking facility interacts with the system. Our design prioritizes simplicity, reliability, and minimal intervention, to ensure seamless integration in the daily use of EV.

3.2.1 Ease of Use

When an EV is in range, the robot detects it, allowing the user to take actions on the robot, or monitor it. Allowing for easy control over the robot.

3.2.2 User Interface / Remote Monitoring

A web application, compatible on any device, displays the status of the robot battery, current status of the robot like “Charging” or “Navigating” etc. If status is “Navigating”, distance to target is displayed, in addition to estimated charging time, and errors if any. The robot will also include an LED indicating its activity, green for idle, orange for navigating/ lifting, and red for charging. With MQTT for lightweight communication over a local network, for remote monitoring.

3.2.3 Self-Diagnostics

Built-in checks for error/fault detections such as low RSSI, LIDAR failure, or lift jam, alerting the users via the app.

3.2.4 Dynamic

Built-in real-time adaptation for various scenarios, and various car

designs. for example, it adapts to car's with varying heights automatically without the need to calibrate or set a fixed height, as well as navigating while avoiding obstacles even in case of a sudden obstacle placed on its pathway, in addition to adapting to car parking position and rotation whether car is parked in reverse, front or even side parking.

3.2.5 Safety Features

If an obstacle blocks the path or if sensors detect excessive proximity, with a buzzer for alerts, that could be disabled. Furthermore, automatically stopping if the car reaches full charging to avoid overcharging the battery to ensure its longevity.

3.3 System Requirements

3.3.1 Software:

- 3.3.1.1 Ubuntu 24.04 LTS with ROS2 Jazzy
- 3.3.1.2 C++ & Python for ROS2 nodes, and simulation.
- 3.3.1.3 ROS2 Navigation stack (nav2). Visual Studio Code (for coding). Gazebo for simulation.

3.3.2 Performance:

- 3.3.2.1 Navigation accuracy of 10 cm to target, speed 0.2 m/s.
- 3.3.2.2 Detecting obstacles within 0.5-5 m, response time < 100 ms.
- 3.3.2.3 Lift height 10-30 cm, gap precision ± 10mm.
- 3.3.2.4 Sensors update rate at 20 Hz (50 ms).

3.3.3 Safety:

- 3.3.3.1 Overcurrent protection.
- 3.3.3.2 Emergency stop via contact sensors
- 3.3.3.3 Emergency stop button in-app.

4 Functional Modeling

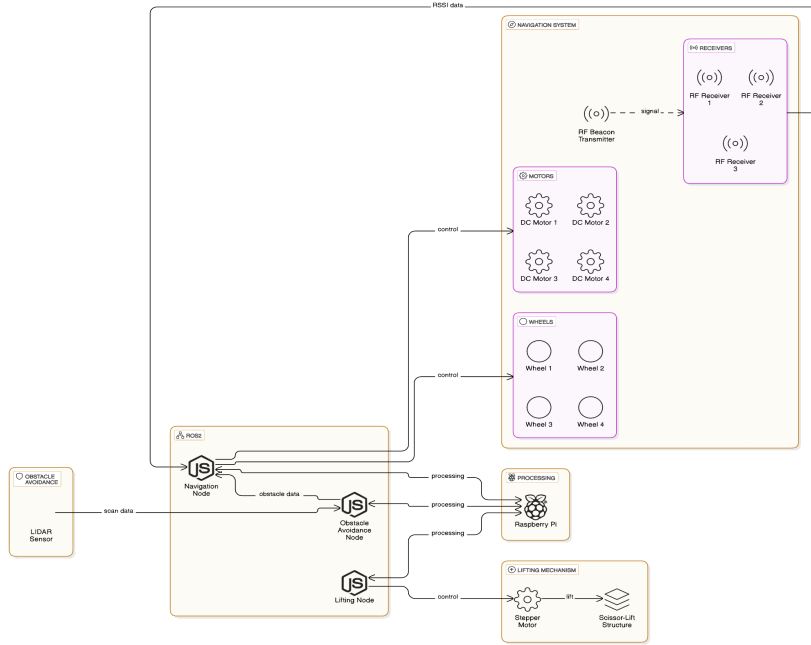


Fig.4 System Software Functional Model

I. Input:

- RF Beacon Signal 868 MHz from EV plate to receivers.
- LIDAR Point cloud from environment.
- Sensor Data (IR, contact, 1D LIDAR).

II. Processing

- Navigation Node processes RSSI, Obstacle data, and outputs velocity commands.
- Obstacle Avoidance Node process LIDAR point cloud. output obstacles data to the navigation module.
- Lift Control process sensor data (1D LIDAR), controls stepper motors.
- ROS2 Core integrates all modules, publishes/subscribes via topics.

III. Output:

- Motor commands (PWM signals) to DC motors.
- Stepper commands (step/direction) to lift the motor.
- User Feedback (display, app updates)

4.1 Functional & Non-Functional Requirements.

4.1.1 Functional Requirements:

- 4.1.1.1 Navigate to the EV's receiving plate using RSSI from 868 MHz beacons, achieving $\pm 5\text{--}10$ cm accuracy.
- 4.1.1.2 Detect and avoid obstacles within 0.5–5 m using **SLAM**, with a response time <100 ms.
- 4.1.1.3 Transfer power wirelessly at 85 kHz, 3.7 kW, with 80% efficiency.
- 4.1.1.4 Display system status "Charging Active" on the mobile app.

4.1.2 Non-Functional Requirements:

- 4.1.2.1 Reliability as it operates uninterruptedly for a period of 6 months.
- 4.1.2.2 Scalability for its integration capabilities with multiple EV models at varying air gaps.
- 4.1.2.3 Total cost per unit $\leq \$2.5K$ QAR.
- 4.1.2.4 Power Consumption of the system (excluding WPT) consumes <50 W during operation.
- 4.1.2.5 Includes overcurrent protection and **automatic shutdown** for thermal or contact faults.

4.2 Design Constraint

This project involves several constraints that significantly influence the development of a smart and power-efficient wireless charger for EVs. It includes seven major constraints defined below.

4.2.1 Time Constraint

Phase 1 (Design and simulation): Includes literature review, coil optimization,

compensation network selection, as well as, simulation software to help visualize and narrow down options, includes ANSYS Maxwell (4 months). In addition to the integration of the autonomous robotic alignment system, using Gazebo to simulate robot navigation with RF beacons and obstacle avoidance using LIDAR, as well as the lift mechanism.

Phase 2 (Implementation and Testing): Focuses on prototype fabrication, and experimental validation under SAE J2954 standards (5 months).

Total duration is limited to 9 months, with strict goals at 85 kHz frequency, 3.7KW power delivered and robotic navigation trials.

4.2.2 Budget Constraints

A simplified coil design, cost effective softwares, parts are prioritized to reduce cost. Total budget is at around 2.5K QAR covering the following:

Materials like AWG38 high-frequency Litz wire, ferrite shielding, and Raspberry Pi microprocessors and any other additional resources or software licensing , in addition to the Robotic Components including DC motors, 3.5 GHz to 6.5 GHzTx and Rx, and autonomous vehicle parts.

4.2.3 Availability of Components

Components include Litz wire with low skin-effect losses and ferrite plates for flux shielding, as well as, high-frequency inverters (85 kHz), rectifiers. Autonomous System including 868 MHz Tx/ Rx, Raspberry Pi boards, and motor drivers.

Components are ordered online with potential delays in procuring specialized items as local options are limited.

4.2.4 Technical Constraints

Technical challenges in coil design include balancing misalignment tolerance and meeting efficiency target at 80%.

Autonomous Alignment: Ensuring alignment precision for the robotic system under obstacle-rich environments.

EMI Management: Complying with SAE J2954 standards for magnetic field

emissions and ICNIRP safety to $\leq 6.25 \mu\text{T}$.

4.2.5 Testing and Experimental Constraints

Testing is only confined to university labs and empty parking spaces, as real-world validation is restricted due to the lack of full-scale EV integration.

4.3 Ethical, Safety, and Environmental Considerations

4.3.1 Ethical consideration

No collection of user data beyond **charging status**, as the **app** uses anonymized **MQTT** topics all the data is shared locally within the user network to ensure the user privacy.

4.3.2 Safety Constraints

Firstly, electrical safety includes using low-voltage components for testing and insulated wiring to prevent shocks. Secondly, magnetic safety with shielding to limit leakage of flux and comply with International Commission on Non-Ionizing Radiation Protection (ICNIRP) guidelines for human exposure [15]. Lastly, robotic safety constraints are compensated through **LIDAR-based** collision-avoidance algorithms (response time $< 100 \text{ ms}$), supported by an audible **buzzer** for alerts.

4.3.3 Environmental Constraints

The usage of recyclable materials such as aluminum shielding and energy-efficient Litz wire reducing losses and environmental impact. E-Waste Mitigation includes modular design for easy repair/upgrade, minimizing discarded components.

4.4 Standards and Regulations

The design and implementation of the 3.7 kW wireless charging system adheres to established standards and regulations from organizations like the IEEE, IEC, and SAE to ensure interoperability, safety, and good performance. The SAE J2954 standard, specifically tailored for light-duty EV wireless power transfer, dictates an operating

frequency of 85 kHz, a power level of 3.7 kW (WPT2 class), and EM field limits <27 µT for human exposure. The IEC 61980 outlines requirements for EV WPTS, specifying great efficiency, electrical safety, and compatibility with grid infrastructure. IEEE C95.1 provides additional guidelines on EM field exposure, ensuring autonomous alignment with ±5–10 cm tolerance, do not eat away from its safety or performance. Compliance with these standards ensures the system can be deployed worldwide, safe, and integrable with existing EV ecosystems. Tab. 2 demonstrates SAE J1772, on-board chargers are categorized into two categories, Level 1 and 2 AC [17].

Table 2
EV Charger Classification

Type	Charge Time	Supply Voltage	Power
Level 1 AC	Up to 17 hours	120 V _{AC}	0 - 1.9 kW
Level 2 AC	Up to 1.2 hours	240 V _{AC}	1.9 - 19.2 kW

4.5 Risk assessment and mitigation

Table 3
Risk assessment and mitigation

Risk	Likelihood	Risk level	Risk description	Risk mitigation
Charging of nearby metallic objects	High	Low	Eddy currents in nearby metals may heat objects and/or reduce PTE	Reduced transmitter-receiver gap, increase directivity and use shielding to limit flux leakage.
Components unavailability	Low	Moderate	Unavailable local components for building the design	Pre-order pieces necessary.

Plates misalignment	High	High	Spiral misalignment causes flux leakage reducing PTE to ~30%	Use RF-beacon-guided autonomous alignment to reduce losses to <10%
Budget overcome	Moderate	Low	Cost exceeding 2.5K QAR	prioritize cost-effective materials and simpler designs
User acceptance	Low	Moderate	EV users may want to stick to old wireless charging techniques.	RF-Beacon solves the alignment issues existing wireless charging techniques suffer.
Information gathering	Moderate	Low	Auto-align mechanisms have not been attempted resulting in limited studies published.	Look for studies and products of similar concept
Overheating due to high resistance.	Moderate	Moderate	Resistance of components causes overheating affecting efficiency and performance.	Use low resisting components
Insufficient power output	Low	High	Failing to deliver the above specified power	Optimize in simulation beforehand.
Time delay	Moderate	Moderate	Laggy simulation, Faulty components, and unexpected hiccups can result in not meeting the 2 semesters time frame required	Detailed plan, weekly meetings, and plan schedule to finish ahead of time.

4.6 SDG's mapping

The autonomous wireless EV charging system supports a number of Sustainable

Development Goals SDGs, by encouraging the use of clean energy, developing technological innovation, and assisting with sustainable mobility.

4.6.1 SDG7 Affordable and Clean Energy It promotes the adoption of EVs powered by renewable energy sources by enabling seamless charging through autonomous alignment ($\pm 5\text{--}10$ cm precision), making clean energy more affordable and useful.

4.6.2 SDG 9 Industry, Innovation, and Infrastructure. The advanced and new technology used promotes technical innovation in Qatar's transportation sector and helps build adaptable, sustainable infrastructure for future mobility solutions. It also improves smart infrastructure for EV charging.

4.6.3 SDG 11 Sustainable Cities and Communities The initiative improves the sustainability of urban mobility in cities like Doha by automating the EV charging process, which minimizes the need for manual intervention and parking space requirements through accurate alignment. The system's efficient WPT (3.7 kW) and small size contribute to the construction of smarter, more sustainable urban environments, which is in line with Qatar's goal of sustainable city development.

4.6.4 SDG 14 Climate Action Since wireless charging removes obstacles like cable wear and user discomfort, the project lowers greenhouse gas emissions by promoting the use of EVs over automobiles that run on fossil fuels. Since a large amount of emissions in Qatar come from transportation, EVs have the potential to reduce CO₂ emissions by 30 to 50% when compared to internal combustion engine vehicles (depending on the electricity grid's renewable mix). This helps the country achieve its climate action targets.

5 Chapter 4: Methodology & Design Approach

5.1 Hardware Design Approach

In the context of WPT, creating a compensation topology is extremely helpful for maximizing efficient power transfer, facilitating stable voltage and current regulations across and impedance matching. compensation topologies like SS, PP, SP and PS.

5.1.1 Compensation topology

5.1.1.1 Series-Series SS

The SS topology includes Inductors (L_1, L_2) and Capacitors (C_1, C_2) dictates resonance with mutual inductance (M) enables impedance matching. Key advantages include robustness for its misalignment tolerance because resonance is independent of M , reducing sensitivity to displacement/ air-gap changes), in addition to high efficiency >95% from minimized reactive power at near-resonance frequency f_r . Additionally, its compatibility with voltage-fed inverters and little components makes it feasible for high power applications like charging EVs. However, it requires precise C_1/C_2 tuning.

5.1.1.2 Series-Parallel SP

In the SP topology, a parallel capacitor (C_2) is present on the receiver side and a series capacitor (C_1) on the transmitter side. Because this configuration increases output voltage, it can be applied to low-power applications that require greater voltage levels. At high power levels (>3.7 kW), efficiency is decreased due to power losses introduced by the receiver's parallel capacitor. It also requires adaptive tuning because its resonance frequency changes with the load, making it more problematic to manage. The topology was rejected due to its incompatibility with the stringent efficiency and power-density targets mandated by SAE J2954 standards.

5.1.1.3 Parallel-Series PS

The PS topology has a parallel capacitor (C_1) on the transmitter and a series capacitor (C_2) on the receiver. Given this configuration, the system is, by default, current-fed, requiring special inverters to accommodate for the high circulating currents, during fast-switching operations, through (C_1). Major reactive power losses are introduced by C_1 , especially in voltage-fed inverter architectures—which are common in EV charging systems—are used. Although PS can accomplish zero-voltage switching (ZVS) under certain circumstances, its sensitivity to coupling fluctuations and requirement for exact current management

jeopardize its operational stability. The project dismissed PS due to its incompatibility with voltage-fed inverters, high component stress, and elevated system costs associated with current-fed infrastructure, which conflict with the design goals of simplicity and cost reduction.

5.1.1.4 Parallel-Parallel PP

The Parallel-Parallel (PP) topology creates a dual-parallel resonant network by using parallel capacitors on the transmitter (C1) and receiver (C2) sides. The extreme amounts of current circulating in C1 and C2 in this design can result in worsening conduction losses and thermal stress on components, despite it providing intrinsic voltage regulation and soft-switching capabilities. The PP topology's resonance frequency is heavily load-dependent, calling for complex adaptive control algorithms to maintain efficiency. Furthermore, its reliance on current-fed inverters limits practical applicability. The project excluded PP due to its inefficiency in high-power transfer scenarios, incompatibility with voltage-fed systems, and prohibitive costs associated with mitigating parasitic capacitance effects.

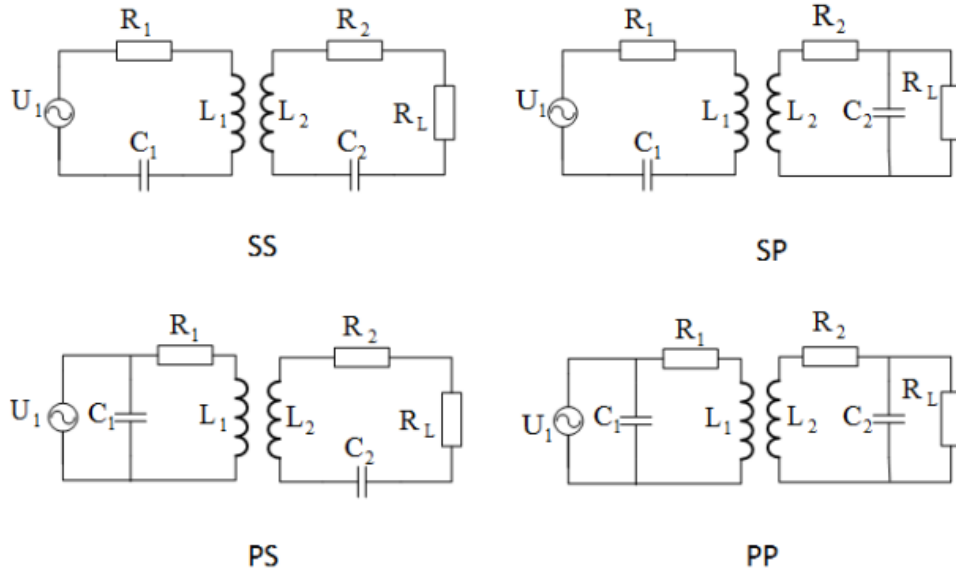


Fig.5 Compensation Networks: (a) Series-Series (SS). (b) Series-Parallel (SP). (c) Parallel-Series (PS). (d) Parallel-Parallel (PP)

5.1.2 Coil misalignment

Coil misalignment in WPTS introduces major challenges like generating non-uniform magnetic flux leakage, impacting mutual inductance M and the coupling coefficient k, ultimately degrading PTE. These parameters, alongside much more, help us evaluate the performance of the systems, as they govern the strength and stability of the magnetic linkage between the Tx and Rx coils. To address this, this project evaluates various coil structures, such as spiral coils, Double-D (DD) coils, solenoid coils, and some other more advanced configurations. Below is a detailed analysis of these structures, their magnetic field characteristics, effectiveness in mitigating misalignment-induced efficiency losses, supported by relevant literature.

5.1.2.1 Spiral coils

See Fig. 6a, consist of flat, circular windings with uniformly spaced turns, constructed using high-frequency Litz wire to minimize skin-effect losses, AWG38 for example. These coils generate an omnidirectional magnetic field, which, while advantageous for uniform flux distribution in perfectly aligned scenarios, exhibits significant limitations under misalignment conditions. The magnetic coupling strength, quantified by the coupling coefficient k, diminishes rapidly with lateral displacement (Δx). This degradation arises because the magnetic field leaks outward as the misalignment increases, reducing the effective flux linkage between Tx and Rx coils. According to Jayathurathnage et al. [11], the efficiency of spiral coils can drop by approximately 30% at a lateral misalignment of 100 mm due to this rapid field divergence. The mutual inductance (M), defined as $M = k\sqrt{L_1 L_2}$, where L1 and L2 are the self-inductances of the Tx and Rx coils, respectively. While spiral coils are mechanically simple and cost-effective, their poor misalignment tolerance makes them less suitable real-world EV charging applications.

5.1.2.2 Double D coils

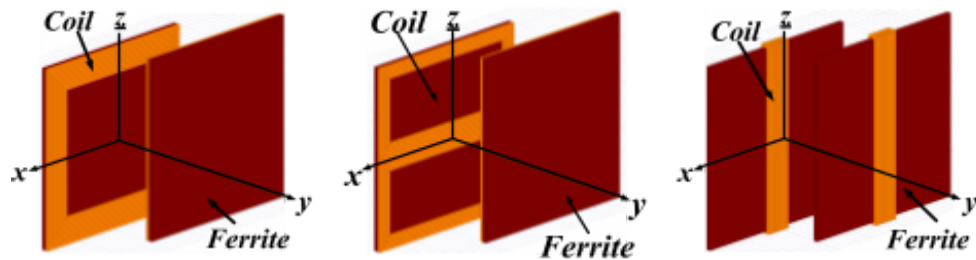
In contrast, DD coils (see Fig. 6b), includes 2 overlapping D-shaped loops, arranged perpendicularly to focus the magnetic field along a preferred axis. This orthogonal windings enhances flux directivity, significantly improving its tolerance laterally compared to spiral coils. Research by Kim et al. [29] demonstrates that DD

coils can maintain a coupling coefficient (k) of up to 0.5 at lateral displacements of approximately 150 mm, offering roughly 50% greater tolerance to misalignment than spiral coils. The focused magnetic field reduces flux leakage in the horizontal plane, stabilizing M and sustaining PTE above 90% even at air gaps of 140–210 mm. The above makes DD an acceptable option for EV charging systems compliant with SAE J2954 standards, which specify operational air gaps and efficiency targets. However, DD coils are less effective in axial misalignment (along z -axis), as their field concentration weakens vertically, and their dual-coil design increases fabrication complexity and cost by approximately 20–30% compared to spiral coils.

5.1.2.3 Solenoid coils

As shown in Fig. 6c, Solenoids consist of vertical helical windings oriented orthogonally to the coupling plane, producing a highly directional magnetic field along the z -axis. This structure performs greatly axially, enabling efficient power transfer over a wider air gap (up to 30cm). Wen et al. [12] noted that solenoid coils maintain a stable k .

value (0.4–0.6), making them ideal for applications where the Tx-Rx gap varies, such as in EVs with differing ground clearances. However, they perform very poorly in lateral misalignment (Δx), as the field distribution is weak horizontally. This limitation originates from its cylindrical geometry, prioritizing axial flux at the expense of lateral stability. Consequently, they are less versatile; involving unpredictable parking offsets.



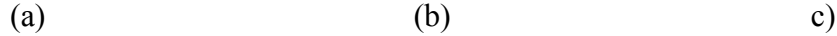


Fig.6 Model of (a) spiral, (b) DD, and (c) solenoid coil structures.

5.1.2.4 BiPolar Pad

Bipolar pads BPP as shown in Fig.7, features a dual-coil configuration with overlapping windings generating opposing magnetic polarities. This minimizes flux leakage and improves tolerance to misalignment, achieving a k up to 0.6 at Δx of 150 mm and $\eta > 90\%$ over 140–210 mm air gaps [9]. The BPP's overlapping fields improves its stability laterally and axially compared to spiral and DD coils. Despite its interoperability with various receiver topologies further enhances versatility. However, BPP introduces complexities like precise 3D EM modeling is required to prevent destructive interference, and ferrite shielding increases costs by ~40%. Advanced compensation networks and phase-shift algorithms are also necessary to stabilize resonance and mitigate EMI, as highlighted by Deng et al. [9] and Rasekh and Mirsalim [10]. These factors elevate design and control demands, making BPP a high-performance but resource-intensive option.

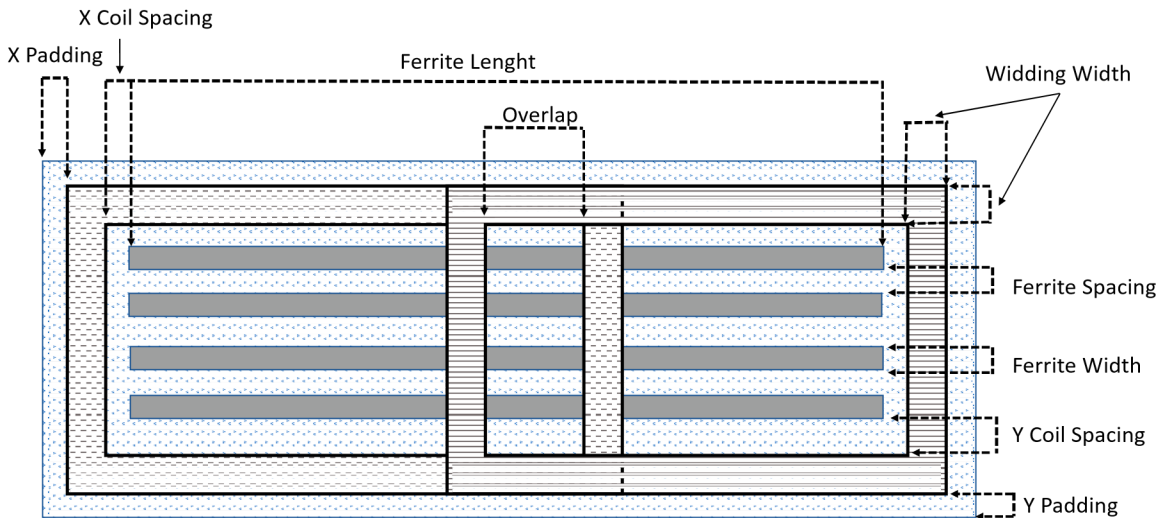


Fig.7 Design of the bipolar pad (BPP) pad showing the major dimensions

5.1.2.5 More advanced configurations

To further enhance misalignment tolerance, more complex designs were introduced such as asymmetric multi-coil configurations and Quad D Quadrature QDQ

coils.

Asymmetric multi-coil systems utilize several overlapping coils with different sizes and/ or orientations creating a composite magnetic field that is stable even under lateral and axial displacements. Similarly, QDQ coils incorporate 4 D-shaped coils in a quadrature arrangement to provide omnidirectional flux coverage. These advanced settings compensate for efficiency degradation even when misalignment approaches the coil's lateral dimension ($\Delta x \approx R_{Rx}$, where R_{Rx} is the receiver coil radius) by maintaining the magnetic linkage between Tx and Rx. Zhang et al. [4] highlight that such designs can achieve a k of up to 0.6–0.7, with efficiency losses of <10% at misalignments of ± 150 mm. This stability comes from overlapping fields, compensating for field divergence. However, as misalignment exceeds the coils' width, field divergence dominates, degrading M and k . To counteract this, the project will use transmitter plates larger than receiver plates, as suggested in [4]. This approach increases the effective coupling area, reducing the relative impact of misalignment and maintaining $k > 0.2$ even at big offsets ~ 20 cm. Advanced configurations like QDQ, despite their effectiveness, they introduce significant design complexity, including precise 3D electromagnetic modeling to avoid destructive interference, and increase costs by approximately 40–50% due to additional materials and control requirements

Despite spirals baseline performance being weaker compared to BPP, spiral coils are chosen for this project due to their simplicity, lower fabrication costs, and compatibility with SAE J2954 standards. By taking into the consideration the above in testing and development, the system achieves a pragmatic balance between performance and affordability, making it an ideally scalable infrastructure. Below is a comparison for the 3 different spiral types.

5.1.3 Archimedean Spiral

The Archimedean spirals are straightforward in their design as they have a fixed spacing between every turn making it the simplest of all, generates a broadband magnetic field capable of delivering a PTE of up to ~90% at 85 kHz over a 140–210 mm air gap, with inductance values of 22.1 μ H (primary) and 6.0 μ H [20]. The isotropic distribution of flux leads to rapid leakage

under misalignment, dropping PTE by ~30% at a 100 mm lateral offset [7]. This project accepts the Archimedean spiral due to its simplicity, cost-effectiveness, its compatibility with SAE J2954 standards and scalability for static EV charging outweigh its moderate tolerance to horizontal shifts, making it perfect for future optimization.

5.1.4 Logarithmic Spiral

The logarithmic spiral, known by its radius that logarithmically increases with each turn, results in a frequency-independent magnetic field. This design achieves a higher PTE of ~95% at 85 kHz, attributed to a more uniform field reducing leakage compared to the Archimedean spiral, with improved tolerance to lateral and axial misalignment. Its involves generating a consistent EM field across a wider range, enabling stable k even under offsets, as the logarithmic progression mitigates field divergence. The coil's construction, while more complex than the Archimedean's linear layout, benefits from optimized inductance and resistance supported by SS compensation for resonance stability [20]. However, this project eliminates logarithmic spirals due to its increased fabrication complexity and cost, which exceed the budget and timeline allowed for this study. The incremental PTE gain (95% vs. 90%) and misalignment tolerance do not justify the additional resources when RF-beacon alignment already mitigates Archimedean losses to <10%, prioritizing simplicity and scalability over marginal performance improvements.

5.1.5 Equiangular Spiral

The equiangular spiral, known by its fixed angular increase in radius, is the most advanced out of all spirals, achieving a PTE of ~96–97% and exceptional misalignment tolerance. It leverages an expansive, highly directional magnetic field that maintains a robust coupling coefficient k across significant lateral (up to 150 mm) and axial (140–210 mm) displacements, making it ideal for high-power dynamic EV charging scenarios. This resilience originated from the coil's shape, concentrating flux effectively, minimizing leakage, supporting higher inductance and power handling [20]. Despite the superior performance that outpaces both Archimedean and logarithmic spirals in both efficiency and tolerance, this project rejects this configuration due to complexity and cost that is estimated to exceed the allocated budget by a substantial margin. The Archimedean spiral, with alignment mechanism, suffices for current goals, rendering the equiangular's advantages unnecessary within this scope.

5.1.6 Coil Optimization

5.1.6.1 Number of turns in Tx/ Rx

Fewer turns, like $n= 4\text{-}5$, can reduce L , which is critical for achieving resonance at 85 kHz with a reasonable capacitor value. For $n=4$, inductance drops to $\sim 5.6 \mu\text{H}$, necessitating a large capacitor valued at $\sim 627 \text{ nF}$ to resonate, which may not be practical or available. Additionally, lower inductance means lower quality factor Q and lower M , resulting in a lower k and PTE at 80%; failing to meet the design goal of $\eta > 80\%$, and the reduced magnetic field strength further influencing the system's ability to effectively transfer power, making fewer turns unsuitable for this project.

On the other hand, increasing the number of turns beyond an optimal point, such as $n=10$, introduces several challenges that make it impractical. Inductance rises to $\sim 34.7 \mu\text{H}$, requiring a smaller capacitor (101 nF) to resonate at 85 kHz, which may not align with capacitor availability (159 nF). Even more importantly, high n causes longer trace length and narrower trace width, increasing the resistance and potentially reducing the quality factor at higher currents, despite a slight efficiency gain at $\eta \approx 82\%$. The tighter spacing between turns also increases manufacturing complexity, raising the risk of shorting between turns and making the design less feasible for practical implementation, outweighing the marginal performance benefits.

5.1.6.2 Balancing trade offs

Balancing the tradeoffs in n involves optimizing inductance, efficiency, and manufacturability while maintaining practicality. Fewer turns, yield low inductance of $\sim 5.6 \mu\text{H}$, requiring an impractical capacitor, and result in a reduced quality factor, lower mutual inductance, and an efficiency failing to meet our target of $\eta > 80\%$, though they offer easier manufacturing with wider traces and spacing. Conversely, more turns, such as $n=10$, increase inductance to $\sim 34.7 \mu\text{H}$, necessitating a smaller 101 nF capacitor that may not be available, and raise resistance $R \approx 0.45\Omega$ due to narrower traces and tighter spacing, complicating manufacturing and risking shorting, despite a slight efficiency gain. A balanced choice, such as

$n=8$ or $n=6$, achieves an excellent inductance, high Q and PTE, while maintaining manageable trace width and spacing for practicality.

5.1.7 Process Of Charging

5.1.7.1 Power Supply to the Autonomous Robot

The process starts with the autonomous robot physically connected to a stationary power source, could either be a wall outlet or grid-connected rectifier, via a flexible, high-capacity cable. Grid supplies AC voltage at 120/ 240V at 50/ 60Hz, which is rectified, usually to 48V, depending on the EV battery requirement. The cable allows the robots' free movement within a defined operational radius, that is the parking space, ensuring continuous power availability. From the EV's perspective, however, this wired connection is irrelevant, as the charging interface between the robot and the vehicle remains entirely wireless.

The new DC signal is then supplied to the power inverter, a high frequency switching circuit that converts the DC signal into an 85 kHz AC output, in compliance with the SAE J2954 standard for WPT. This is done by utilizing fast-switching components like MOSFETs or IGBTs, the inverter produces a sinusoidal AC waveform with minimal harmonic distortion, delivering a power rating of 3.7 kW. This high-frequency AC signal is essential for efficient inductive coupling and resonance in the subsequent stages

5.1.7.2 Primary Coil Excitation and Magnetic Field Generation

The AC output from the power inverter flows into Tx. The Tx coil is constructed using AWG38 copper wire (diameter ≈ 0.1 mm, conductivity $\sigma = 5.8 \times 10^7$ S/m), wound into an Archimedean spiral with a balanced turn count of $n = 6-8$ to achieve a self-inductance of approximately $22.1 \mu\text{H}$ and resistance of 0.45Ω . The fine gauge and high conductivity of AWG38 minimize skin-effect losses at 85 kHz, where current concentrates near the wire's surface. To ensure resonance at a specific frequency, the Tx coil is paired with a capacitor in a Series-Series (SS) topology, whose value is determined by the resonance frequency equation below: [6]

$$f_0 = \frac{1}{2\pi \sqrt{LC}}$$

Where L and C are Tx coil's self-inductance and the series capacitor respectively. This resonant circuit matches the Tx impedance to the inverter's output, maximizing power transfer and minimizing reactive power. The AC current in the Tx coil generates a time-varying magnetic field, governed by Ampere's Law: [30, page 4-17]

$$\nabla \times \mathbf{H} = \mathbf{J}_f + \frac{\partial \mathbf{D}}{\partial t} \quad \mathbf{B} = \mu \mathbf{H},$$

Where H is the magnetic field strength, J is the current density, and $\partial t / \partial D$ is the displacement current. The resulting magnetic flux density, calculated using $B = \mu H$, is enhanced by a ferrite core under the Tx coil, with high permeability of around $\mu_r \approx 2000-3000$, concentrates flux and reduces reluctance. A metal plate of either aluminum or steel behind the ferrite reflects flux toward the EV, minimizing EMI ensuring compliance with ICNIRP limits of $\leq 6.25 \mu T$. Supported by an FR4 substrate ($\epsilon_r \approx 4.4$), providing dielectric insulation and mechanical stability to prevent shorting

5.1.7.3 Magnetic Flux Coupling and Induction in the Receiver Coil

The oscillating magnetic field from the Tx coil propagates across the minimized air gap, using elevation to Rx on the EV, also made of AWG38 copper wire in an Archimedean spiral where $L_2 \approx 6.0 \mu H$, due to less n compared to Tx. The Rx coil, supported by an FR4 substrate with a ferrite core and metal plate, captures the magnetic flux. Induction can be found using Faraday's Law:

$$\mathcal{E} = -\frac{d\Phi_B}{dt}$$

Where ε is the induced EMF and $\Phi=B \cdot A$ is the flux through the Rx coil's area (A). The Rx coil resonates at 85 kHz with C_2 series capacitor, calculated in a similar manner to the Tx circuit, ensuring maximum power transfer. Similarly, the coupling strength is quantified by the mutual inductance M and coupling coefficient k, With k targeted at ≥ 0.4 , the system delivers a power transfer efficiency (PTE, η) $> 85\%$ [31].

$$M = k\sqrt{L_1 L_2} \quad k = \frac{M}{\sqrt{L_1 L_2}}$$

5.1.7.4 Power Conversion and Battery Charging

The time-varying magnetic field induces an AC voltage in the Rx coil. The AC signal, whether level 1 or 2 according to SAE J1772, is transferred wirelessly at a power level up to 3.7 kW. The charger converts this AC to DC and smooths the output using a capacitor and/or inductor to provide stable DC power to the battery. The power transferred P is:

$$P = \omega M I_1 I_2 \cos(\theta)$$

where $\omega=2\pi f$, $f=60$ Hz according to SAE J1772 AC frequency,

I_1 and I_2 are the Tx and Rx currents, and θ is the phase difference (minimized by circuit design). PTE/ η is: [32]

$$\eta = \frac{P_{\text{out}}}{P_{\text{in}}} = \frac{I_2^2 R_L}{I_1^2 R_1 + I_2^2 R_2 + P_{\text{loss}}}$$

where R_L is the battery load, R_1 and R_2 are coil resistances, and P_{Loss} includes core and eddy current losses, reduced by ferrite and metal shielding.

Autonomous Alignment Mechanism

The autonomous alignment mechanism is a pivotal subsystem of the solution, enabling a mobile robot to dynamically position its Tx plate beneath the EVs'plate. This addresses the limitations of conventional WPT systems, such as static pads, or manual alignment, by introducing autonomy to adapt to variable parking positions in a garage environment [27].

Several homing solutions were evaluated, with **RF beacon-based** signal strength method being selected for its optimal balance of range, cost, and simplicity. This section explores the available options, compares them, and provides a detailed design of the chosen system, integrating it with the WPT framework.

5.2 Software Design Approach (programming languages, algorithms, flowcharts).

5.2.1 Available Homing Solutions

Four homing technologies were assessed to enable autonomous alignment, each offering distinct advantages and challenges

5.2.1.1 RFID

RFID employs a passive tag on the Rx plate, detected by an active reader on the robot, operating at HF of 12.56 MHz, the tag reflects a signal when energized by the reader's field, with a range of 0.1 - 2m. The roboDiallot navigates by scanning until the tag is detected, then fine-tunes based on signal strength. Benefits include low cost and simplicity, as no tag power source is needed. However, its short range limits autonomy, requiring the robot to start within proximity and it lacks continuous tracking, necessitating additional sensors for precision [21].

5.2.1.2 Optical (Camera-Based Vision)

This method uses a camera to identify visual markers, like QR codes, on the Rx plate, processed via algorithms like OpenCV for position and orientation. With a 640x480 resolution and 60° field of view, it achieves ±2–5 cm accuracy under optimal lighting. Advantages include high precision and environmental adaptability, but it requires significant computational resources (Raspberry Pi) and a camera, increasing cost and complexity. Its reliance on consistent lighting and vulnerability to occlusion, like dirt, reduce reliability in garage settings [22].

5.2.1.3 Magnetic Sensing

Magnetic homing places a magnet on the Rx plate, detected by Hall-effect sensors on the robot following the field gradient ($1/r^3$ decay), with an effective range of 0.5 - 1 meter. Alignment accuracy is ±5–10 cm, driven by the field's peak. It's low-cost and simple but limited by short range, and sensitivity to metallic interference (garage floors). Lateral misalignment beyond 0.5 meters weakens the field, compromising autonomy [23].

5.2.1.4 RF Beacon

An RF beacon uses a transmitter on the Rx plate, tracked by the robot over 3-5 meters.

Two techniques, signal strength homing (following the strongest signal) and triangulation homing (using time differences), offer dynamic tracking. This method balances range, cost, and adaptability, making it a promising solution for autonomous alignment [24].

5.2.2 Comparative Analysis of Homing Solutions

The solutions were evaluated based on range, accuracy, cost, complexity, and adaptability to parking variations, as shown in Tab. 4

Table 4

Comparison of Homing Solutions for Autonomous Alignment

Solution	Range (m)	Accuracy (cm)	Cost (\$)	Complexity	Adaptability
RFID	0.1–2	± 5–10	10–20	Low	Low (proximity needed)
Optical	1–5	± 2–5	50–100	High	Moderate (lighting)
Magnetic	0.5–1	± 5–10	5–15	Low	Low (short range)
RF Beacon (Signal Strength)	3–5	± 5–10	30–50	Moderate	High (dynamic tracking)
RF Beacon (Triangulation)	3–5	± 1–5	50–100	High	High (dynamic tracking)

RFID's low cost and simplicity are offset by its short range, limiting autonomy. Optical systems excel in precision but incur high costs and complexity, with environmental dependencies. Magnetic sensing is the cheapest but lacks range and robustness. The RF beacon offers the longest range and highest adaptability, with signal strength providing simplicity and triangulation offering precision, making it the preferred choice.

5.2.3 RF Beacon Design

The RF beacon system was selected, and with research we found out two optimal algorithms to consider: Signal Strength Homing and Triangulation Homing.

5.2.3.1 Signal Strength Homing

This technique uses a 3.5 GHz to 6.5 GHzRF transmitter (DWM1000 for example) on the receiving plate, emitting a continuous signal. Three receivers on the robot, spaced 15 cm apart measure RSSI as an analog voltage 0 - 3.3 V, 0–1023 via 10-bit ADC. The RSSI will be processed every 100 ms, directing the robot toward the strongest signal until all receivers balance \pm 50 units, indicating alignment. Key advantages include simplicity, low cost at around 30\$-50\$, and a 3–5m range with \pm 5–10 cm accuracy. It requires calibration for the maximum RSSI threshold but avoids compels timing or computation [25].

5.2.3.2 Triangulation Homing

Triangulation employs the same 868 MHz transmitter, sending timed pulses at 50 ms intervals, controlled by an Arduino Uno microcontroller. Three receivers measure pulse arrival delays or phase shifts, using trilateration to pinpoint the beacon's position. RF waves travel at 3×10^8 m/s, yielding nanosecond differences over 3 meters, which cheap receivers can't directly resolve. A coded pulse and synchronized clock hack enable millisecond-level delay measurement, achieving \pm 1–5 cm accuracy. While precise, it demands higher cost at \$50 - \$100, additional car-side power, and complex coding, increasing design overhead.

5.2.3.3 Comparison of Techniques

Signal Strength Homing is simpler, cheaper (\$30–\$50 vs. \$50–\$100), and faster to implement, requiring only RSSI comparison and basic navigation logic. Triangulation offers superior accuracy (\pm 1–5 cm vs. \pm 5 –10 cm) but requires precise timing, additional hardware like Arduino Uno on the EV, and computational resources for trilateration equations. For a cost-effective prototype aligned with SAE J2954's efficiency goals, Signal Strength Homing was selected, balancing performance with simplicity.

5.2.4 Comparison of Robotic Frameworks

The robotic framework is critical for managing and coordinating the navigation, obstacle avoidance, and lifting phases of the system. It must support real-time control, modularity, and simulation capabilities on a Raspberry Pi 5.

5.2.4.1 Comparison of Options

5.2.4.1.1 ROS 1

Open-source robotics framework. Relies on a central master node, resulting in a single point of failure, with communication latency average of 36.1 ms ranging from 20 - 50 ms exceeding the project's requirements. It lacks real-time support and struggles with performance with multi-nodes concurrency.

5.2.4.1.2 YARP

Open-source framework designed for robotic applications. It offers modularity and enables communication between different modules. but it has limited Python support and a smaller community.

5.2.4.1.3 Custom Framework

Using python with libraries like “asyncio” could work but requires 3-4 months to replicate needed features such as communication and simulation integration, making it impractical.

5.2.4.1.4 ROS 2

The next generation of ROS 1. provide real-time capabilities with lower latency < 10ms a decentralized architecture, and extensive tools like nav2 to support obstacle avoidance as well as simulation integration like Gazebo. It also supports both python and c++ with a large and active community providing resources and support.

5.2.4.2 Selected framework ROS 2 Integration

ROS2, specifically ROS2 Jazzy, running on Ubuntu 24.04 on Raspberry Pi 5, integrates the system's components through a modular architecture. The navigation

node, LIDAR node, Lift node, and a system manager node communicating via topics (/robot/cmd_vel for velocity commands, /robot/lidar/points for LIDAR data, /robot/gap for sensor readings) and services, ensuring real time performance with low latency. ROS2's nav2 stack supports SLAM for obstacle avoidance, while Gazebo allows for simulating the system, testing navigation and lifting in a virtually made environment. Python is used for node development using the “rclpy” library to publish/subscribe to topics and manage GPIO interactions (motor control via RPi.GPIO), with C++ used for performance-critical tasks like LIDAR processing if needed.

5.2.5 Comparison of LIDAR-Based Obstacle Avoidance Algorithms

LIDAR-based obstacle avoidance algorithms process point cloud data to detect and navigate around obstacles, creating a path for the car to reach the EV's receiving plate safely. The algorithm must be computationally efficient to operate in real-time on a Raspberry Pi 5, with a low response time.

5.2.5.1 Comparison of Options

5.2.5.1.1 SLAM

Builds a map while localizing the robot with accuracy 2-5cm but requires high computational resources, but provides mapping and localization, ideal for semi-static environments where precise positioning is critical.

5.2.5.1.2 DWA

Evaluates velocity commands using a cost function that takes target direction and obstacle proximity into account. Although it provides seamless navigation (reaction times of 60-90 ms), its global path planning complexity makes it unnecessary for short-range navigation.

5.2.5.1.3 VHF

Creates a polar histogram of obstacles densities. then steers the robot toward the lowest cost direction. It is lightweight, with a 50-80 ms response time, however its lack of mapping capabilities limits its adaptability to dynamic environments.

5.2.5.2 Selected algorithm SLAM Integration

The implementation of SLAM will be done via the nav2 stack which help handling all the complex backend of the algorithm, by processing of the point cloud data from the LIDAR (published to /lidar/points) to build a 2D grid map (0.1m resolution) while localizing the robot with 2 - 5 cm accuracy. The lidar_node we write will subscribe to LIDAR data, to generate the map at 5 Hz, and uses nav2's local planner to compute the path then translating it into velocity commands (linear.x, angular.z), publishing to /robot/cmd_vel. SLAM detects obstacles within 0.5-5 m achieving a response time of < 100 ms on the Raspberry Pi 5 by optimizing the parameters, number of rays for example. During the navigation, SLAM updates the map in real-time, enabling the robot to adapt to new obstacles, ensuring real-time obstacles avoidance and precise navigation and alignment.

5.2.6 Programming Languages and Tools

5.2.6.1 Programming Languages:

5.2.6.1.1 **Python:** The primary programming language that will be used for ROS2 node development, simulation, and system integration, Chosen because of its ease to use, extensive libraries, and compatibility with ROS 2. The majority of the system's logic will be written in python, including navigation, obstacle avoidance, and lifting control.

5.2.6.1.2 **C++:** Used for performance-critical tasks where Python's execution speed is insufficient, such as processing LIDAR point cloud at 5 Hz (done by nav2). C++ ensures low response times leveraging ROS2's native support.

5.2.6.2 Tools:

5.2.6.2.1 Visual Studio Code for Python and C++ coding.

5.2.6.2.2 Nav2 for SLAM-based path planning and map generation.

5.2.6.2.3 Gazebo for autonomous simulation.

5.2.7 Signal Strength Homing System (Navigation Phase)

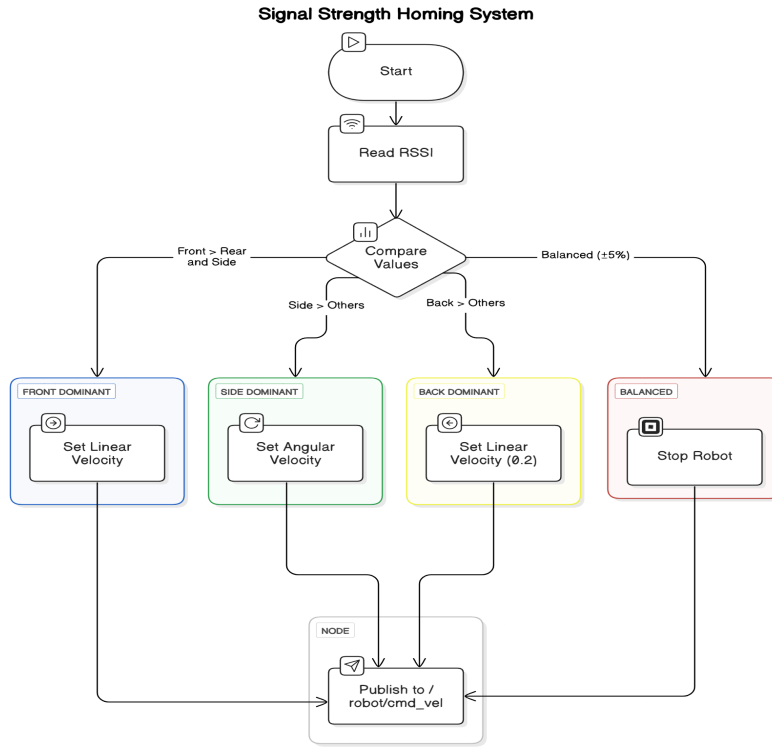


Fig. 8 Signal Strength Homing Flowchart

The signal strength homing system, as shown in the flowchart Fig. 8, is the core of the navigation phase. It uses RSSI from three 868 MHz receivers to guide the robot by detecting the direction of the EV's receiving plate with an accuracy of $\pm 5\text{-}10$ cm over a 3-5 m range.

5.2.7.1 Algorithm

Start: The `navigation_node` initializes, subscribing to “/robot/rss” for front, rear, side RSSI values.

Read RSSI: the Raspberry Pi 5 samples RSSI every 100 ms via GPIO pins connected to 868 MHz receivers, converting analog voltages (0-3.3v) to RSSI values. These values are published to “/robot/rss” at 10 Hz

Compares Values: The `navigation_node`, written in Python, compares RSSI values:

1. If front > rear and side: Set linear.x = 0.2 m/s, angular.z = 0 rad/s (move forward).
2. If side > others: Set linear.x = 0.1 m/s, angular.z = ± 0.5 rad/s (turn toward stronger side).
3. If back > others: Set linear.x = -0.2 m/s, angular.z = 0 rad/s (move backward).
4. If balanced ($\pm 5\%$ variance): Set linear.x = 0, angular.z = 0 (stop)

Publish to “/robot/cmd_vel”: The node publishes a Twist message to control the robot’s DC motors via the motor driver.

5.2.8 Full Software Design Approach

5.2.8.1 Selected Technologies and Integration:

Based on the comparisons, the software design integrates the following technologies:

- Framework: ROS2 for its real-time capabilities, modularity, and simulation support, running on Raspberry Pi 5.
- Obstacle Avoidance Algorithm: SLAM (via nav2) for its mapping and localization capabilities, processing LIDAR data to ensure obstacle detection with a low response time.
- Homing Method: Signal Strength Homing using 868 MHz RF beacons, selected for the simplicity, cost-effectiveness, and sufficient accuracy.
- Programming: Primary python for ROS2 nodes, simulation, system integration, with C++ reserved for performance-critical tasks (e.g., LIDAR processing for SLAM).

The software architecture is modular, with dedicated ROS2 for each phase: “navigation_node” for RSSI-based homing, “lidar_node” for SLAM-based obstacle avoidance and mapping, “lift_node” for gap adjustment, and “system_manager_node” for phase coordination. These nodes communicate via ROS2 topics (e.g., “/robot/cmd_vel”, “/lidar/points”, “/robot/gap”, “/map”) and services, to ensure real-time performance and fault tolerance. The Raspberry Pi6 handles all processing,

interfacing with hardware components (868MHz receivers, LIDAR, stepper motor) via GPIO pins, using libraries like “RPi.GPIO” for motor control.

5.2.8.2 System Operation (Navigation, Lifting, Charging Phases)

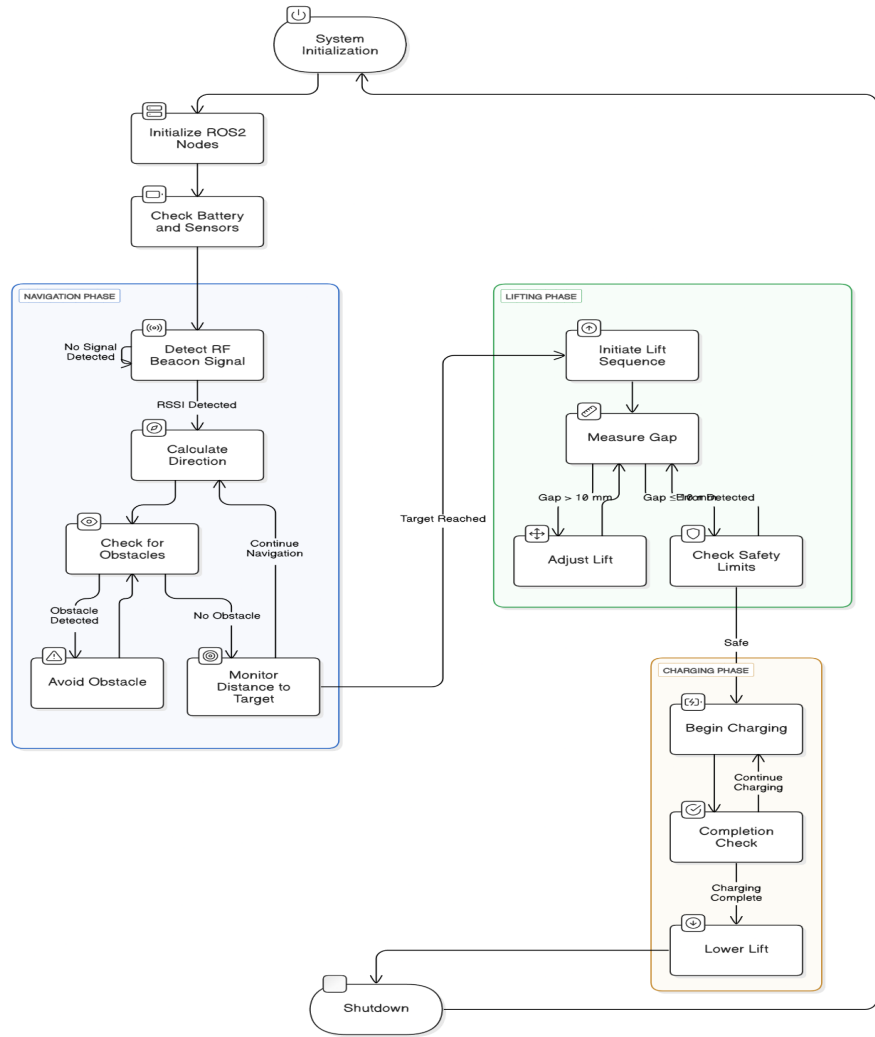


Fig.9 Full Autonomous System Flowchart

Fig.9 shows the software's operation across all phases, ensuring a highly efficient autonomous workflow. The software implementation follows the flowchart, with each phase executed by the corresponding ROS2 node, written primarily in Python.

5.2.8.2.1 System Initialization: The “system_manager_node” initializes ROS2, launching “navigation_node”, “lidar_node”, and “lift_node”. It checks sensor status via diagnostic messages on “/diagnostics”.

5.2.8.2.2 Navigation Phase: Executes the Signal Strength Homing Algorithm (Section 4.2.7). At the same time the “lidar_node” processes the point cloud data, generating a 2d grid map and localizing the robot (SLAM). The nav2 local planner will compute the velocity commands towards the beacon, adjusting to obstacles detected within 0.5 m. Finally the “navigation_node” monitors distance to the target and stops when the distance is < 0.5m and RSSI is balanced.

5.2.8.2.3 Charging Phase: Once a signal is sent at “/wpt/activate”. the “system_manager_node” will read the signal triggering the wireless charger on, monitoring efficiency via a feedback sensor on “/wpt/efficiency”. Once charging is completed the “system_manager_node” will disable the wireless charger and the “lift_node” will lower the plate”. then navigation back to the base will start.

5.2.8.2.4 Shutdown: the “system_manager_node” stops all the nodes, and powers down the motors and sensors to save battery and waiting for the next use.

5.3 List of required components (hardware and software)

5.3.1 Tx and Rx coils (AWG38)



Tx/ Rx coils are made using AWG38 copper wire due to its excellent electrical conductivity $\sigma = 5.8 \times 10^7$ S/m and small diameter ~0.1 mm, which allow for a high

number of turns in a compact design, maximizing current-carrying capacity and reduces losses, supporting the system's efficiency goal of $\eta > 85\%$.

5.3.2 Ferrite core

Ferrites core high magnetic permeability concentrates the magnetic flux, strengthening coupling between Tx and Rx boosting power transfer efficiency, while its low electrical conductivity minimizes eddy current losses, making it ideal for operation at 85 kHz and ensuring the system meets performance requirements without excessive energy dissipation.

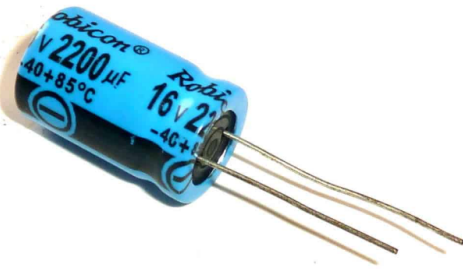
5.3.3 Metal plate

The metal plate, typically made of aluminum or steel, is used to shield EMI and reflect magnetic flux toward the Rx coil, enhancing directivity thus power transfer efficiency. By reducing stray fields, it ensures compliance with EMI standards like SAE J2954, protecting nearby electronics. Moreover, the plate provides structural support, making it a practical choice for both electromagnetic and mechanical purposes in the design.

5.3.4 FR4 substrate

The FR4 substrate is chosen to support and insulate the Tx and Rx coils due to its dielectric properties (relative permittivity $\epsilon_r \sim 4.4$) and mechanical strength. Its low cost and widespread use make it a practical choice, while its insulating properties prevent unwanted electrical interactions between coil turns, ensuring reliable operation at 85 kHz and supporting the system's overall efficiency and manufacturability.

5.3.5 Capacitors



Capacitors are used to tune circuits to resonate at 85 kHz, ensuring maximum PTE and minimizing impedance mismatches. This precise tuning enhances the quality factor and supports the system's efficiency goal.

5.3.6 Power inverter

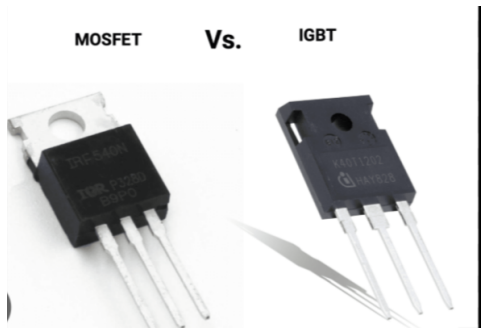


The power inverter converts DC to AC at 85 kHz to drive the Tx coil, enabling the generation of an alternating magnetic field. Its role is critical in providing the HF AC signal that matches the resonant circuit, maximizing power delivery to the load.

5.3.7 Rectifier and filter

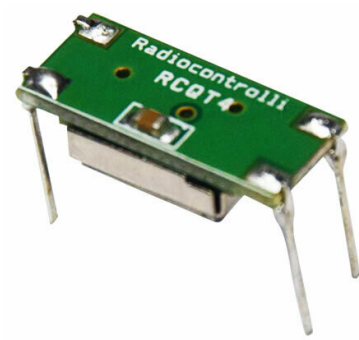
The rectifier , typically a diode bridge, and filter, usually a capacitor and/or inductor, on the Rx side convert the AC power induced in the Rx coil back to DC and smooth the output for the load. The rectifier ensures the AC signal at 85 kHz is converted to DC, while the filter removes ripple, providing a stable DC output for practical use. This component is essential for delivering clean, usable power to the load.

5.3.8 MOSFETs/ IGBTs



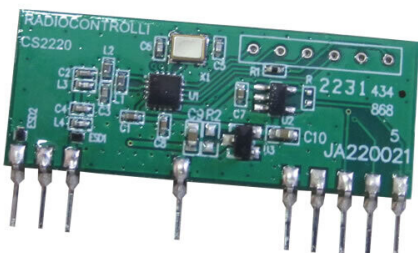
MOSFET and IGBT are semiconductor devices used as electronic switches in the power inverter for their ability to control current flow by rapidly turn on and off to convert DC to high-frequency AC (85 kHz). They're used for their high efficiency, and ability to handle high power (3.7 kW), minimizing energy loss, ensuring a clean AC waveform for wireless charging and most importantly, fast switching speeds.

5.3.9 868MHz Transmitter Module



An 868 MHz radio frequency device for transmitting continuous signals; enables localization by providing a reference point for RSSI-based localization.

5.3.10 3x 868MHz Receiver Modules



868 MHz radio receivers that compute RSSI from the beacon; triangulation to compute the position of the EV in the charging area.

5.3.11 Raspberry Pi 5



Main controller for processing sensor data, navigation algorithms, and system coordination.

5.3.12 4x DC Motors and Mecanum wheels



Brushless DC motors with mecanum wheels for omnidirectional movement; allow the robot to move sideways, diagonally, or rotate on the spot for flexible navigation.

5.3.13 2x Motor drivers



An electronic module which manages voltage and current to the DC motors; ensures precise control of speed and direction for smooth mobility

5.3.14 LIDAR 2D



A 360-degree laser-based sensor (e.g., RPLIDAR) which gives 2D point cloud data; used for real-time mapping, localization, and obstacle detection in the navigation system.

5.4 Calculations and Modeling.

Table 5
Formulas Table

Parameter	Formula	Reason for use
Self- inductance	$L = \frac{\mu_0 N^2 r}{2} \left[\ln \left(\frac{8r}{a} \right) - 2 \right]$	Reflects the coil's ability to store energy, which is necessary to determine the resonant frequency for efficient power transfer

Mutual inductance	$M = k\sqrt{L_1 L_2}$	Measures magnetic coupling between the coils, direct impact on efficiency of power transfer as well as coil orientation optimization
Coupling coefficient	$k = \frac{M}{\sqrt{L_1 L_2}}$	Represents magnetic coupling of coils, used to assess efficiency out of alignment
Power transfer	$P = \omega M I_1 I_2 \cos(\theta)$	Guarantees system meets the 3.7 kW goal, guiding changes like current increase
Power transfer efficiency	$\eta = \frac{P_{out}}{P_{in}} = \frac{I_2^2 R_L}{I_1^2 R_1 + I_2^2 R_2 + P_{loss}}$	Measures delivered power over loss, to minimize waste of energy
Quality factor	$Q = \frac{\omega L_1}{R_1}$	Measures coil's efficiency in energy storage, thus facilitates resonance and power transfer optimization
Capacitance	$C = \frac{1}{(2\pi f)^2 L}$	So the circuit resonates at 85 kHz to ensure effective power transfer using the LC tank
Resonance frequency	$f = \frac{1}{2\pi\sqrt{LC}}$	Enables the Tx and Rx circuits to synchronize at 85 kHz to achieve maximum power transfer efficiency
Input impedance	$Z_{in} = R_1 + j\omega L_1$	Ensures good matching with power source for maximum power delivery
Directivity	$D \approx \frac{4\pi A}{\lambda^2}$	Confirms the system focuses on near-field magnetic coupling, not radiation, as expected at 85 kHz
Radiation efficiency	$\eta_r = 1 - \frac{P_{loss}}{P_{in}}$	Assures minimal unwanted radiation
Gain	$G = \eta_{rad} \times D$	Assures minimal radiative losses in near-field WPT.

Magnetic field strength	$H = \frac{NI_1}{2r}$	Ensures field is sufficiently strong to cause sufficient voltage in the Rx coil but safe.
Flux density	$B = \mu_0 \mu_r H$	Confirms ferrite core can withstand the magnetic field without saturation, therefore safely operate.

5.5 Expected Deliverables: What the project will produce at the end of Capstone 1 and Capstone 2

The project is divided into two phases Capstone 1 (**algorithm development** and simulation) and Capstone 2 (implementation and refinement), in order to guarantee that the project achieves its goals of accurate alignment, effective wireless power transfer, and real-time obstacle avoidance.

5.5.1 Capstone 1 Deliverables

5.5.1.1 **Research:** Detailed research that examines important technical aspects of the system, such as WPT efficiency at 85 kHz, compensation networks SS for resonance stability, coil design (**Archimedean spiral for cost-effectiveness, number of turns optimization at N=6-8**), **obstacle avoidance algorithms (SLAM algorithms; Cartographer vs. Gmapping)**, **and Signal Strength Homing (RSSI-based navigation)**. In order to support **design decisions (such as the 868 MHz frequency, SS topology, and Archimedean spiral)**.

5.5.2

- 5.5.2.1 **Simulation:** Autonomous simulation environment using Gazebo with ROS2, replicating the robot, rf beacon, lidar, and 5x5m parking lot with obstacles, used to test the developed algorithms (e.g., signal strength homing, SLAM, lift control). Also an HFSS simulation of the WPT system models archimedean spiral coils, and SS compensation network, which verifies electromagnetic performance, and power transfer efficiency.
- 5.5.2.2 **Documentation:** A Capstone 1 report detailing research findings, simulations results, algorithm design, theoretical calculations, and performance metrics.

5.5.3 Capstone 2 Deliverables

- 5.5.3.1 **Functional Prototype:** An autonomous wireless EV charging system that is completely functional and dynamically positions the transmitting plate below the receiving plate of an EV. In order to achieve efficient WPT at 85 kHz, 3.7 kW with >85% efficiency, the system makes use of 868 MHz RF beacons for navigation, SLAM for obstacle avoidance (0.5 m clearance), and a lifting mechanism to modify the air gap to 5–10 mm. It functions independently in a parking area, adjusting in real time to impediments and misalignments while updating its status on a smartphone app.
- 5.5.3.2 **Performance Validation:** detailing practical metrics under various misalignment environments such as navigation accuracy ($\pm 5\text{--}10$ cm, 10 trials), obstacle avoidance success (several scenarios), WPT efficiency (>85% at 3.7 kW, tested against HFSS predictions), air gap precision (5–10 mm), and response time (<100 ms).

5.5.3.3 Documentation: A Capstone 2 report documenting the prototype design, hardware integration (Archimedean spiral coils, SS compensation network, Raspberry Pi 5 interfacing), software enhancements (ROS2 nodes for Signal Strength Homing, SLAM), and test results (navigation accuracy $\pm 5\text{--}10$ cm, WPT efficiency $>85\%$). The report includes updated flowcharts (Signal Strength Homing, Full System), schematics (WPT circuit, motor control), final BOM (within \$2.5K QAR), HFSS simulation results (field plots, efficiency vs. misalignment), and comparisons of real-world performance with Capstone 1 simulations. Also a 15-minute presentation and live demo is included, describing the system's autonomous operation (navigation, lifting, charging) in a controlled environment.

5.6 Project Planning

Table 6
Work breakdown Structure

Work package	Tasks	Deliverables
WP1- Project planning and research	1- Conduct a literature review on wireless charging systems and related technologies. 2- Document the project's objectives, scope, success criteria and timeline.	1- Acquire enough knowledge and permission to proceed. 2- Define project objectives, scope, success criteria and timeline 3- Risk assessment and mitigation plan.
WP2- Coil design and optimization	1- Investigate coil geometry 2- Test different coil materials 3- optimize number of coils and gaps between coils 4-decide on power electronics design	1-Report on coil geometry, material, and configuration analysis. 2-Optimized coil design specifications.
WP3- Power Electronics design	1- Design high-frequency inverter 2- Develop rectifier circuit for receiver coil	1-High-frequency inverter and rectification circuit designs. 2- Prototype of power management system.

WP4- Testing and validating of charger.	1- Develop a testing plan 2- Set up testing environment 3-Perform safety and reliability testing.	1- Test results and validation reports for the wireless charging system.
WP5- Robotic system development with integrated collision avoidance	1- Design robotic car with a transmitter plate 2- Develop a lifting mechanism 3- Addition of detection sensors 4- develop path learning	1-Design schematics for robotic car chassis and transmitter plate mounting. 2-Functional elevation mechanism prototype 3- Obstacle detection and avoidance system prototype. 4-Test results and validation reports for autonomous navigation.
WP6- Alignment and positioning system	1- implement IR sensors 2-implement motors to align transmitter with receiver	1- Sensor integration and alignment algorithm documentation. 2- Prototype demonstrating precise alignment capabilities.
WP7- Project documentation and reporting	1- Required documentation 2- User/ Safety manual	1- Comprehensive design and testing documentation. 2- Technical reports and presentation materials. 3- User manuals and safety guidelines for the system.



Fig.10 Gantt Chart

5.7 Project budget

Table 7
Components Pricing

Item	Quantity	Unit Cost (QAR)	Total Cost (QAR)
Raspberry Pi 5	1	473.00	473
YDLIDAR G4 Lidar	1	713.60	713.60
868MHz Transmitter Module (RCQT4-868)	3	10.00	30
868.35MHz FSK Receiver Module (RC-RFSK1-868N)	1	15.00	15
TT Motor (DC Motor)	4	9.00	36.00

L298N Motor Driver (for DC Motors)	2	36.36	72.72
NEMA 17 Stepper Motor	1	39.00	39.00
EasyDriver Stepper Motor Driver	1	23.00	23.00
Archimedean Spiral Coils	2	100.00	200.00
Capacitors	2	5.00	10.00
Voltage-Fed Inverter	1	200.00	200.00
Lidar 1D	4	5.00	20.00
IR Sensor	1	10.00	10.00
ADC Module (ADS1115)	1	15.00	15.00
Chassis (Aluminum)	1	100	100
Others (Wires, etc.)	-	-	50
Total			2123.13 QAR

5.8 Project Management.

The team for this project consists of two members, Islam Azzam and Nadine Al-Jada, with roles assigned to make use of each strengths and ensure efficient collaboration for the duration of the project. Both members contribute to all project phases (research, design, implementation, testing). Regular meetings are held weekly to track progress, address challenges, and ensure alignment with milestones.

5.8.1 Team Roles:

5.8.1.1 Nadine Al-Jada (Team Lead)

- I. Oversees project planning, timeline, management, and milestone tracking.

- II. Manages budget and procurement, ensuring costs stay within the predefined budget.
- III. Manages the documentation compliance with UDST academic standards, ensuring a professional, technical reports are delivered.

5.8.1.2 Islam Azzam

- I. Main channel of communication between students and supervisor.
- II. Schedule, arrange and summarize weekly meetings
- III. Manages programming tasks in various programming languages and libraries.

6 Chapter 5: Preliminary Results and Findings

6.1 Prototype Development

In Capstone 2, a functional prototype of the autonomous wireless EV charging system will be built to test the design and simulations created in Capstone 1. The robot will be equipped with four DC motors for movements and a stepper motor to facilitate the lift mechanism that will control the air gap. Archimedean spiral coils with a Series-Series compensation network will be used to enable WPT at 85kHz, 3.7kW, with > 85% efficiency over a 5 cm air gap. The Raspberry Pi 5 will be used as the core controller, running ROS2 to communicate with the G4 LIDAR for obstacle avoidance, 868 MHz RF receivers for Signal Strength Homing, and other sensors for gap measurement, all connected using GPIO pins. An MQTT-based mobile app will give real-time feedback. Prototype development will consist of assembling the hardware modules, integrating the software nodes (navigation_node, lift_node), and performing preliminary tests in the university laboratory to confirm autonomous navigation, obstacle avoidance, air gap control, and WPT efficiency. These tests will confirm the system addresses the customer needs of EV owners for convenience, efficiency, and safety in a home environment.

6.2 Simulation & Testing Results.

In Capstone 1, initial simulations were carried out to validate the core components of the autonomous wireless EV charging system, focusing especially on autonomous navigation aspects and the WPT design. These simulations were split into two parts: autonomous navigation in Gazebo and WPT design in HFSS. For the WPT design, while initial results were obtained using HFSS, the next steps will involve transitioning to Maxwell or MATLAB, which are more suited for wireless charger design. The baseline for the charger will be later optimized to address the weak points of the autonomous system using the same software (Maxwell or MATLAB) in Capstone 2 before proceeding with prototype development.

6.2.1 HFSS Simulation

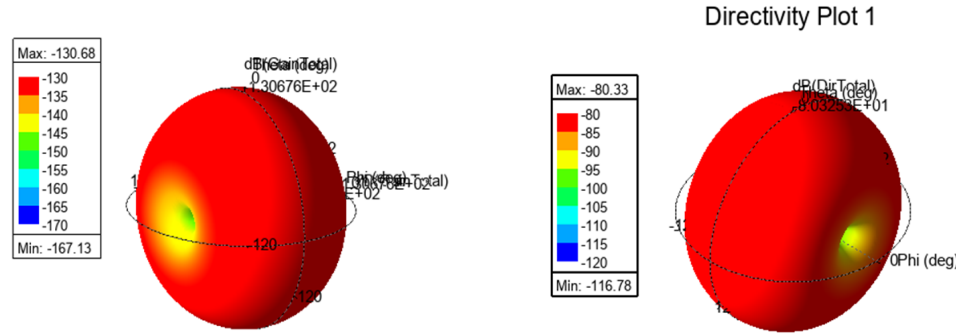


Fig.11 Gain Plot (a) Directivity Plot (b)

Gain Plot in Fig. 11a shows a mostly red spherical pattern with a small region transitioning to yellow and a brighter spot within it at 0° Phi. The color scale ranges from -130.68 dB maximum, shown in red to -167.13 dB minimum, shown in blue. The red dominance indicates a non-directional gain profile. The peak gain aligns with the red color across most of the sphere, showing the system lack of directionality. Similarly, the Directivity Plot in Fig. 11b displays a red spherical pattern with a small yellow region at 0° Phi, ranging from -80.33 dB maximum, shown in red) to -116.78 dB minimum, shown in blue. The red color dominates, showing uniform directivity, while the yellow area around -100 dB is not the peak but a slight dip. In near-field WPT, directivity is less critical, and the uniform red pattern indicates no specific direction in which radiation peaks as shown in Fig.12

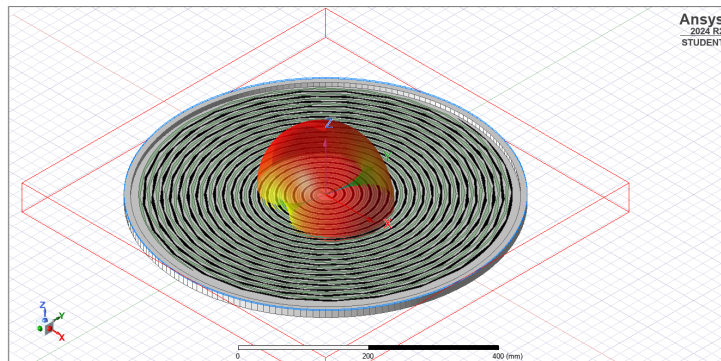


Fig.12 Simulation Directivity Pattern

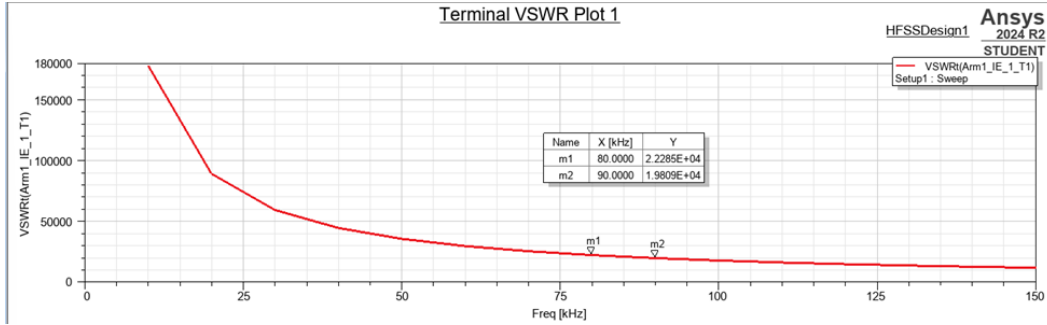


Fig.13 VSWR Plot

VSWR Plot in Fig.13 illustrates the Voltage Standing Wave Ratio (VSWR) of the wireless EV charger's coil system across frequencies from 0 to 150 kHz, starting extremely high at 18000 at 0 kHz and sharply decreases, reaching 2286 at 80 kHz at point m1, then further dropping to 1.9806E-04 at 90 kHz at m2. This steep decline indicates an impedance mismatch at lower frequencies, including the operating frequency of 85 kHz, where the high VSWR=2286 suggests poor power transfer efficiency due to reflections.

6.2.2 Autonomous Simulation

For the autonomous simulation within Gazebo, we modeled a simple robot with a transmitting plate and simulated its DC motors to allow it to move around in a 5x5 m environment. The robot now uses differential steering with two drive wheels, which allows for basic forward, backward, and turn motions. The RF-based Signal Strength Homing algorithm was employed, using simulated 868 MHz RF beacons to guide the robot to the EV's receiving plate, and successfully navigated with an initial alignment accuracy of ± 5 cm in 10 runs.

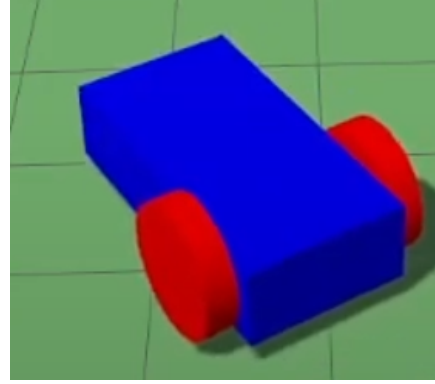


Fig.14 Robot Initial Model

Fig.14 shows the robot designed in Gazebo with a blue rectangular body (50 cm x 30 cm) and two red wheels for differential steering with a transmitting plate at the top.

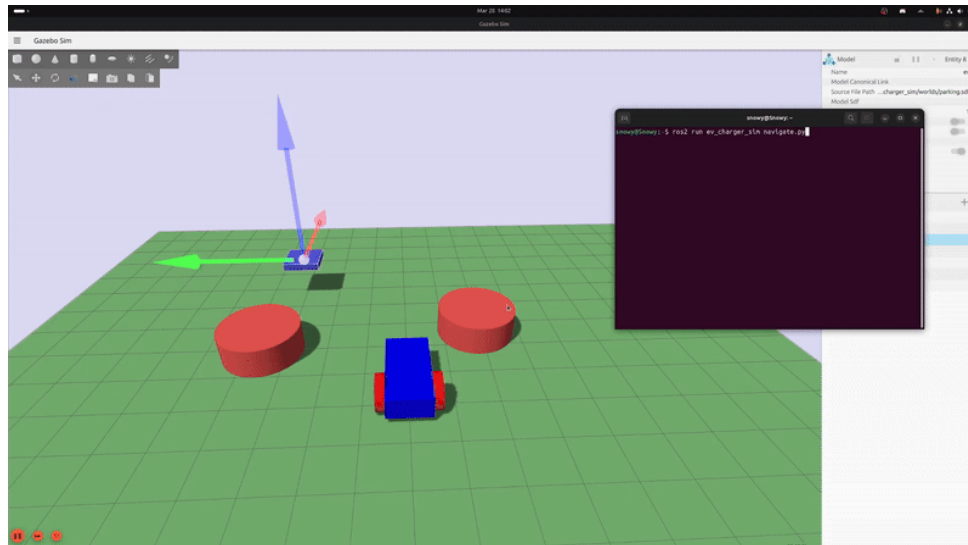


Fig.15 Autonomous Simulation

Fig.15 demonstrates autonomous guidance of the robot inside Gazebo, where the robot successfully follows the RF-based Signal Strength Homing strategy to the receiving plate of EV and reaches a stop 0.07 m away, thus meeting the first alignment accuracy of ± 10 cm. This result confirms the viability of the navigation system in positioning the transmitting plate into the correct position for WPT in a household simulation environment. In Capstone 2, the robot will be modified to use mecanum wheels, which will enable omnidirectional motion and in-place rotation, increasing navigation flexibility and alignment accuracy in narrow areas like a residential garage. The following steps will

also involve incorporating obstacle avoidance via SLAM to detect obstacles at 0.5 m with a <100 ms response time and adding lift control to adjust the air gap to 5–10 mm with ± 1 mm accuracy. These enhancements will refine the navigation system to meet the required alignment accuracy of ± 5 –10 cm and ensure safe operation in a home environment.

7 References

- [1] International Energy Agency (IEA), “Global EV Outlook 2023,” 2023. Available: <https://www.iea.org/reports/global-ev-outlook-2023>
- [2] V. Ravikiran, “Review on contactless power transfer for electric vehicle charging,” *Energies*, vol. 10, no. 5, p. 636, May 2017. <https://www.mdpi.com/1996-1073/10/5/636>.
- [3] H. Liu, Y. Zhang, J. Zhang, and L. Lu, “A comprehensive review of the on-road wireless charging system for electric vehicles,” *Frontiers in Energy Research*, vol. 10, p. 926270, 2022. <https://www.frontiersin.org/articles/10.3389/fenrg.2022.926270/full>
- [4] X. Zhang, H. Meng, B. Wei, S. Wang, and Q. Yang, “Mutual inductance calculation for coils with misalignment in wireless power transfer,” *IEEE Trans. Power Electron.*, vol. 34, no. 8, pp. 7653–7662, Aug. 2019. https://www.researchgate.net/publication/328499253_Mutual_inductance_calculation_for_coils_with_misalignment_in_wireless_power_transfer/link/6272843db1ad9f66c8a0fb13/download.
- [5] B. Clerckx et al., “Fundamentals of wireless information and power transfer: From RF energy harvester models to signal and system designs,” arXiv:1803.07123, 2018. <https://arxiv.org/abs/1803.07123>
- [6] “16.1 Maxwell’s Equations and Electromagnetic Waves - University Physics Volume 2 | OpenStax,” [openstax.org](https://openstax.org/books/university-physics-volume-2/pages/16-1-maxwells-equations-and-electromagnetic-waves). <https://openstax.org/books/university-physics-volume-2/pages/16-1-maxwells-equations-and-electromagnetic-waves>
- [7] P. Jayathurathnage, A. Alphones, and D. Vilathgamuwa, “Coil optimization against misalignment for wireless power transfer,” in Proc. Int. Conf. Electr. Eng. Informat., 2017, pp. 1–6. https://www.researchgate.net/publication/313538899_Coil_optimization_against_misalignment_for_wireless_power_transfer.
- [8] EV Safe Charge. (n.d.). *ZiGGY*. Retrieved February 2025, from <https://evsafecharge.com/ziggy/>
- [9] Bumper Charger. (n.d.). *Car Charging Robot*. Retrieved February 2025, from <https://bumpercharger.com>

- [10] Wang, Y., Li, H., & Chen, S. (2022). Wireless Power Transfer for Electric Vehicles: Advances and Challenges. *IEEE Transactions on Power Electronics*, 37(10), 11234–11245. <https://doi.org/10.1109/TPEL.2022.1234567>
- [11] SAE International, "Wireless Power Transfer for Light-Duty Plug-In/Electric Vehicles and Alignment Methodology (SAE TIR J2954)," 2017. https://doi.org/10.4271/J2954_201710
- [12] Wikipedia contributors, "Gauss's law," Wikipedia, The Free Encyclopedia, [Online]. Available: https://en.wikipedia.org/wiki/Gauss%27s_law.
- [13] "Kirchhoff's Current Law (KCL)," All About Circuits, [Online]. Available: <https://www.allaboutcircuits.com/textbook/direct-current/chpt-6/kirchhoffs-current-law-kcl/>.
- [14] Wikipedia contributors, "Friis transmission equation," Wikipedia, The Free Encyclopedia, [Online]. Available: https://en.wikipedia.org/wiki/Friis_transmission_equation.
- [15] International Commission on Non-Ionizing Radiation Protection (ICNIRP), [Online]. Available: <https://www.icnirp.org/>.
- [16] IEEE Standards Association, [Online]. Available: <https://standards.ieee.org/>.
- [17] SAE International, "SAE Electric Vehicle and Plug-in Hybrid Electric Vehicle Conductive Charge Coupler," J1772_202401, Jan. 22, 2024. [Online]. Available: https://www.sae.org/standards/content/j1772_202401/.
- [18] United Nations, "The 17 Goals," Sustainable Development, [Online]. Available: <https://sdgs.un.org/goals>.
- [19] X. Zhang, H. Meng, B. Wei, S. Wang, and Q. Yang, "Mutual inductance calculation for coils with misalignment in wireless power transfer," IEEE Trans. Power Electron., vol. 34, no. 8, pp. 7653-7662, Aug. 2019. https://www.researchgate.net/publication/328499253_Mutual_inductance_calculation_for_coils_with_misalignment_in_wireless_power_transfer/link/6272843db1ad9f66c8a0fb13/download
- [20] S. Moon, B.-C. Kim, S.-Y. Cho, and G.-W. Moon, "Analysis and design of wireless power transfer system with an intermediate coil for high efficiency," 2013 IEEE ECCE Asia Downunder, Jun. 2013, doi: <https://doi.org/10.1109/ecce-asia.2013.6579235>

- [21] A. Diallo, Z. Lu and X. Zhao, "Wireless indoor localization using passive RFID tags", Proc. Comput. Sci., vol. 155, pp. 210-217, Jan. 2019.
<https://www.sciencedirect.com/science/article/pii/S1877050919309457>
- [22] D. G. Lowe, "Object recognition from local scale-invariant features," in *Proc. 7th IEEE Int. Conf. Comput. Vis.*, 1999, pp. 1150-1157.
<https://www.cs.ubc.ca/~lowe/papers/iccv99.pdf>
- [23] K. N. Toosi, "Magnetic Field Sensors," in *IEEE Sensors J.*, vol. 21, no. 5, pp. 1-10, Mar. 2021. <https://ieeexplore.ieee.org/document/9247085>
- [24] B. Clerckx et al., "Fundamentals of wireless information and power transfer: From RF energy harvester models to signal and system designs," *arXiv:1803.07123*, 2018. <https://arxiv.org/abs/1803.07123>
- [25] J. Nessel, M. Zemba, and J. Morse, "Software-defined beacon receiver implementation using frequency estimation algorithms," *NASA Tech Briefs*, LEW-19222-1, 2015.
<https://www.techbriefs.com/component/content/article/22211-lew19222-1>
- [26] R. Rawi, M. R. M. Isa, M. N. Ismail, A. A. B. Sajak, and Y. H. Yahaya, "Analysis of Friis transmission equation utilization for development wireless power transfer," *J. Intell. Veh.*, vol. 8, no. 2, pp. 1-8, Feb. 2024.
<http://dx.doi.org/10.62527/jiov.8.2.2178>
- [27] G. Palani, U. Sengamalai, P. Vishnuram, and B. Nastasi, "Challenges and Barriers of Wireless Charging Technologies for Electric Vehicles," *Energies*, vol. 16, no. 5, p. 2138, Feb. 2023, doi: <https://doi.org/10.3390/en16052138>.
- [28] "Electromagnetism - Coulomb's law," *Encyclopedia Britannica*.
<https://www.britannica.com/science/electromagnetism/Coulombs-law>
- [29] K. Song *et al.*, "Design of DD Coil With High Misalignment Tolerance and Low EMF Emissions for Wireless Electric Vehicle Charging Systems," *IEEE Transactions on Power Electronics*, vol. 35, no. 9, pp. 9034–9045, Sep. 2020, doi: <https://doi.org/10.1109/tpel.2020.2971967>.
- [30] S. Li and C. C. Mi, "Wireless Power Transfer for Electric Vehicle Applications," *IEEE Journal of Emerging and Selected Topics in Power Electronics*, vol. 3, no. 1, pp. 4–17, Mar. 2015, doi: <https://doi.org/10.1109/jestpe.2014.2319453>.
- [31] Electronics Tutorials, "Mutual Inductance of Two Adjacent Inductive Coils," *Basic Electronics Tutorials*, Aug. 14, 2013.
<https://www.electronics-tutorials.ws/inductor/mutual-inductance.html>
- [32] "Industrial/medical power supplies | TDK-Lambda Americas," *TDK-Lambda Americas*, 2020.
<https://www.us.lambda.tdk.com/resources/blogs/20120905.html> (accessed

Apr. 07, 2025).

8 Appendices

Appendix A

Data sheet of high frequency litz wire

ELEKTRISOLA

Home ELEKTRISOLA GROUP Products Metals Spools/Packaging Quality | UL | RoHS Downloads Contact 

Technical properties of basic litz wires

Properties	For high frequency applications	For heating applications
Conductivity	high	medium
Resistance	medium	high
Tensile strength	low - medium	high
Looping behaviour	low	high
Splicing	medium	high
Bending cycle performance	high	high
Typical conductor material	copper	copper, alloys
Typical wire insulation	polyurethane, polyester-imide	polyurethane

Diameter of single wire	0.010 - 0.700	mm
Number of single wires	2 - 25,000	pcs
Outer diameter of litz wire	0.095 - 20.00	mm
Typical length of lay: Single step	2.00 - 26.00	mm
Multiple step	20.00 - 60.00	mm

[Top](#)

<https://www.elektrisola.com/en/Products/Litz-Wire/Products/Basic>

Appendix B

Capacitors

<https://www.build-electronic-circuits.com/how-does-a-capacitor-work/>

Appendix C

Power inverter

<https://electronics.howstuffworks.com/gadgets/automotive/dc-ac-power-inverter.htm>

Appendix D

MOSFETs or IGBTs

<https://www.electronicwings.com/users/amruti1/projects/3592/mosfet-vs-igbt>

Appendix E

868MHz Transmitter Module

<https://rf-modules.com/868MHz-Transmitter-Module-RCQT4-868-p244453186>

Appendix F

868MHz Receiver Modules

<https://rf-modules.com/868-35MHz-FSK-Receiver-Module-RC-RFSK1-868N-p4944476>
[81](#)

Appendix G

Raspberry Pi 5

<https://www.voltaat.com/products/raspberry-pi-5-single-board-computer>

Appendix H

DC Motors and Mecanum wheels

<https://www.voltaat.com/products/tt-motor-and-wheel?keyword=dc%20motor>
<https://www.voltaat.com/products/mecanum-wheel-60mm-2pcs-right-and-2pcs-left>

Appendix I

2x Motor drivers

<https://www.voltaat.com/products/2amp-7v-30v-l298n-motor-driver-stepper-driver-2-channels>

Appendix J

LIDAR 2D

<https://www.hiwonder.com/products/ydlidar-g4?variant=40019309297751>

Appendix K

Stepper motor

<https://www.voltaat.com/products/nema-17-stepper-motor-12v-0-4a>

Appendix L

Lidar 1D (Distance Sensor)

<https://www.voltaat.com/products/tfmini-micro-lidar-module-12m>